Naval Research Laboratory

Washington, DC 20375-5320

NRL/MR/6350--19-9827

Influence of Electric Current on the Mechanical Deformation of Metals

Christopher C. Rudolf, Won Mo Kang*, Christopher J. Kindle**,
Siddiq M. Qidwai**, Chandra Pande and James P. Thomas

Multifunctional Materials Branch
Materials Science and Technology Division

**ASEE Postdoctoral Associate*
***Former Naval Research Laboratory Employee*

February 27, 2019

REPORT DOCUMENTATION PAGE

Form Approved
OMB No. 0704-0188

1. REPORT DATE *(DD-MM-YYYY)*	2. REPORT TYPE	3. DATES COVERED *(From - To)*
27-02-2019	Memorandum Report	October 2016 - September 2018

4. TITLE AND SUBTITLE

Influence of Electric Current on the Mechanical Deformation of Metals

5a. CONTRACT NUMBER

5b. GRANT NUMBER

5c. PROGRAM ELEMENT NUMBER
61153N

6. AUTHOR(S)

Christopher C. Rudolf, Won Mo Kang*, Christopher J. Kindle**, Siddiq M. Qidwai**, Chandra Pande and James P. Thomas

5d. PROJECT NUMBER

5e. TASK NUMBER

5f. WORK UNIT NUMBER
63-4993-08

7. PERFORMING ORGANIZATION NAME(S) AND ADDRESS(ES)

Naval Research Laboratory
4555 Overlook Avenue, SW
Washington, DC 20375-5320

8. PERFORMING ORGANIZATION REPORT NUMBER

NRL/MR/6350--19-9827

9. SPONSORING / MONITORING AGENCY NAME(S) AND ADDRESS(ES)

Office of Naval Research
One Liberty Center
875 North Randolph St., Suite 1425
Arlington, VA 22203

10. SPONSOR / MONITOR'S ACRONYM(S)
ONR/NRL

11. SPONSOR / MONITOR'S REPORT NUMBER(S)

12. DISTRIBUTION / AVAILABILITY STATEMENT

DISTRIBUTION STATEMENT A: Approved for public release; distribution is unlimited.

13. SUPPLEMENTARY NOTES

*Former ASEE Postdoctoral Associate in the Multifunctional Materials Branch
**Former Employees in the Multifunctional Materials Branch

14. ABSTRACT

This report describes novel experiments developed to characterize electron-dislocation interactions in um/nm-scale specimens via in situ transmission electron microscopy (TEM) and tensile deformations of mm-scale specimens with applied electric currents and cooling that decoupled Joule heating from the current. The TEM results showed no apparent electron-dislocation interactions at current densities up to 5000 A/mm2 with single-crystal Cu, and the coupled-tensile testing results showed large current effects on the plastic deformation of polycrystalline Ti but no effects with Cu and Fe.

15. SUBJECT TERMS

Electroplasticity, electrically assisted deformation of metals, thermo-electro-deformation coupling, crystal plasticity, dislocation dynamics

16. SECURITY CLASSIFICATION OF:			17. LIMITATION OF ABSTRACT	18. NUMBER OF PAGES	19a. NAME OF RESPONSIBLE PERSON
a. REPORT	b. ABSTRACT	c. THIS PAGE			James P. Thomas
Unclassified Unlimited	Unclassified Unlimited	Unclassified Unlimited	Unclassified Unlimited	46	19b. TELEPHONE NUMBER *(include area code)* (202) 404-8324

Standard Form 298 (Rev. 8-98)
Prescribed by ANSI Std. Z39.18

This page intentionally left blank.

CONTENTS

LIST OF FIGURES

LIST OF TABLES

This page intentionally left blank.

EXECUTIVE SUMMARY

In recent years, researchers have shown many interesting and advantageous effects of the concurrent application of low-density electric current (tens to hundreds of A/mm^2) on the formability of metals. Elimination of springback, reductions in flow stresses, and enhancements in strains-to-failure have been demonstrated for various pure metals and alloys under uniaxial loading conditions. The potential benefits of electrically-assisted metals processing give rise to the need for understanding this phenomenon at the fundamental material scales (nano and micro) and the development of analytical (theoretical and computational) tools.

There is no currently established understanding of the effect of electric current on material deformation mechanisms. Two mechanisms have been proposed: 1) joule heating effects, and 2) the electroplasticity effects (electron interaction with dislocations). Historically, both originated in response to experiments from the 1970s and 80s that used high-amperage, short-duration current pulses (most ac, $\sim 10^3$-10^8 A/mm^2; $<10^{-5}$ s) applied with mechanical loading. However, interpretation of these early results was difficult due to the dynamic, transient effects of the coupled fields. Experimental characterization with lower density constant currents in smaller scale specimens was performed to develop further understanding on this topic by the Multifunctional Materials Branch of the Naval Research Laboratory (NRL) under the Core 6.1 Research Program (Work Unit # 63-4993).

This report provides an overview of the findings from basic research performed under this program including: 1) development of a new experimental capability for characterizing electron-dislocation interactions in μm/nm-scale specimens via in situ transmission electron microscopy (TEM); 2) results for pure, single-crystal copper samples showing no apparent electron-dislocation interactions at large constant current densities (several thousand A/mm^2); 3) development of a new experimental facility for characterizing the tensile deformation behavior of mm-scale specimens with constant applied currents and effective specimen cooling to achieve uniform conditions in the gage section (strain, current density, and temperature) that effectively decouples Joule heating effects from electric current effects; and 4) experimental results for pure, polycrystalline copper, iron, and titanium specimens showing significant current effects on the plastic deformation of the titanium, but no observed effects with the copper and iron.

The results from 1) & 2) are addressed in Chapter 2 and were reported in more detail in several journal publications referenced therein. The results from 3) & 4) are addressed in detail in Chapter 3 and Appendices A & B. A journal paper reporting on the meso-scale research will be submitted soon for publication.

ACKNOWLEDGEMENTS

WK and CR were supported on this project through American Society for Engineering Education Postdoctoral Fellowships at NRL. This work was supported by the Office of Naval Research (ONR) through the US Naval Research Laboratory's Basic 6.1 Research Program.

This page intentionally left blank.

CHAPTER 1: INTRODUCTION

Traditional metal forming of bulk sheet and plate metals requires machinery capable of applying large forces to complex tool and die hardware to shape the materials to a desired 3D geometry through plastic deformations. Metal forming requires high power and consumes large amounts of energy, and the large forces needed to plastically deform the metal feedstock necessitates tooling that can handle the metal-forming forces without deforming excessively and without significant wear. Lowering the loads associated with metal forming would reduce the power/energy consumed and allow for the use of less costly tooling with reduced wear during forming.

Techniques for reducing the base-metal flow stress and increasing the ductility would enable increases in metal forming efficiency and capability (shape-complexity). In this regard, forming at higher temperatures would be a suitable option if not for the added process complications and forming hardware, which often render it non-viable.

Research studying the effects of electric polarization or current flow on the plastic deformation behavior of conductive and non-conductive materials began in the late 1950's. With metals specifically, the effects of high-density current pulses or low-density dc currents on the plastic deformation behaviors and properties have been investigated in detail [1-10]. In recent years, researchers have shown many interesting and advantageous effects of the concurrent application of low-density electric current (10^1-10^2 A/mm^2) on the formability of metals that can be utilized to markedly improve material processing techniques involving bulk or localized deformations. Complete elimination of spring-back, reductions in flow stresses of up to one order of magnitude, and enhancements in strains-to-failure by up to eight times have been demonstrated for various pure metals and alloys under uniaxial loading conditions (e.g., [1, 5]).

Two primary mechanisms have been proposed for the observed electric effects: 1) Joule heating; and 2) electro-plasticity (e.g., electron interaction with dislocations). Historically, both mechanisms originated from experimental studies conducted in the 1970s and 80s with high-amperage, short-duration current pulses (~10^3-10^8 A/mm^2; <10^{-5} s; mostly ac) applied concurrently with mechanical deformation [11]. However, the interpretation of material responses from those experiments has proven to be difficult due to the transient (dynamic) effects of the coupled thermal, electrical and mechanical fields [2]. The overreliance on bulk-scale observations (e.g., [2, 3, 11]) has likely been a detriment to better understanding of the nature of the electrically assisted deformation (EAD) of metals.

> *The objective of this research was to develop and perform experiments to isolate and assess the effects of dc electric current on the tensile deformation behavior of high-purity copper, iron, and titanium representing the three primary metal crystal structures: face-centered cubic (fcc), body-centered cubic (bcc), and hexagonal-close packed (hcp).*

The critical experimental challenge was decoupling the effects of joule heating from electric current on the observed plastic deformation behavior. To address this challenge, two key requirements for the experiments were set: 1) the distribution of mechanical strain, electric

Manuscript approved February 27, 2019.

current density, and temperature within the specimen gage section must be uniform; and 2) load-deformation experiments with matched "applied-current" gage-section temperatures must be conducted to provide baselines for assessing pure thermal effects on the deformation behavior. Unambiguous interpretation of the experimental results requires uniform conditions in the gage section. Many of the experiments reported in the literature have specimen geometry and fixturing features that may produce localized stress/deformation, current, and/or temperature concentrations in the gage section, and localized field concentration in the gage section can easily lead to erroneous conclusions from the experimental results.

In this work, two novel experimental capabilities were developed for characterizing the coupled electro-thermo-mechanical behavior of metal samples under tensile loading with an impressed dc current. The first system was developed for in situ transmission electron microscope (TEM) experimentation on μm-scale specimens. It employed a commercial loading stage fitted with custom Si micro-device fixturing and specimen designs for concurrent deformation-current testing in the TEM. The specimen gage section was 10 x 10 x 0.1 μm in dimension. The large surface to volume ratio (~20) in the gage section and the short gage length enables rapid dissipation of the joule heat via radiative transport and conduction into the TEM sample holder so that high current densities (~>10^3 A/mm^2) were possible with minimal increases in specimen temperature. The first-generation device did not include force measurement. The current design includes a force transducer, however, fabrication and testing with force measurement has not been completed. As a consequence, the TEM results included in this report are qualitative consisting of direct observations of dislocation motion with applied strains and currents.

A second system was developed for experimentation on mm-scale specimens (meso-scale). It employed a commercial scanning electron microscope (SEM) mechanical loading stage made for in situ SEM mechanical testing. Custom modifications were made to the device to safely enable large current flows through the mounted test specimens. Forced-air convection with vortex cooling was used to maintain uniform (surface) temperature conditions within the gage section. Non-contact video strain and IR temperature measurements were employed. Test control, and measurement data acquisitions were all computer automated. A parallel testing approach was also developed employing a laboratory materials test system with an environmental chamber for temperature control. This system was used to characterize the load-deformation behavior of specimens under similar temperature conditions as the applied current tests, as a baseline for assessing the electric current contributions to the deformation response.

This report is organized into two main Chapters. The first reports on the in situ TEM experiments on pure Cu single-crystal specimens. Several publications on this work have already appeared, so this Chapter is more of a summary. The second (Chapter 3) reports on the meso-scale SEM experiments and results for polycrystalline Cu, Fe, and Ti specimens. This Chapter includes many details and results. A related journal paper will be submitted for publication soon. The report concludes with a highlight of the important results and recommendations for future studies. An Appendix provides more details on the preliminary meso-scale test system designs.

CHAPTER 2: MICRO/NANOSCALE CHARACTERIZATION

A micro-device testing method that utilizes the unique advantages of micro/nanotechnology was developed for in situ investigations of the coupled electromechanical behavior of metals. Electron-dislocation interplay in single crystal copper (SCC) was directly investigated using this in situ capability with a focus on electroplasticity with minimal Joule heating effect. In this chapter, the micro-device testing method, key results, and brief conclusions are provided. Additional details on this part of the work can be found in references [12-14].

Micro-Device Testing Method

The micro-device has three main components: an electrically insulated (SiO_2-coated) Si frame, a dog-bone shaped specimen, and silver wires (Figure 1a). The frame is designed to prevent inadvertent mechanical loading of the specimen during handling/operations and to fit onto a commercial electromechanical TEM holder (Gatan Model 654, single tilt straining holder). Silver wires are connected on one end to the electrical feedthrough from the TEM holder and on the other to the sample, which itself is attached to the frame with an Ag epoxy. The micro-device is fixed on one end and the other can be pulled in nominal displacement control. This particular device offers several advantageous features: 1) in situ electromechanical TEM capability, 2) ability to achieve high (~10^3 A/mm^2) current density owing to the submicron-size specimen cross-section, 3) uniform electrical current and nominal stress, up to the small strain limit, in contrast to traditional TEM specimens, and 4) effective thermal management [12-14].

The first feature provides an opportunity to directly observe the movement of dislocations due to electric current, if any. The required current to achieve high specimen current densities is minimal (mA's) because of the small cross-section area. The third feature is critical in simplifying the analysis of the operative deformation mechanisms. The last feature is invaluable because it permits independent observation of electron-dislocation interactions due to effective radiative and conductive heat-transfer that mitigates Joule heating in the vacuum environment. For a given desired electric current density, the required supply current and the Joule heating scale by the square and cube of the characteristic specimen length, respectively. Joule heating is very small in micron-scale specimens. Analytical and numerical simulations show that for a pure Cu sample with a gage length of 10 μm and a cross-section of 100 nm x 10 μm, 5 mA of current corresponds to 5000 A/mm^2 of current density and an estimated 8.33 μW of Joule heating that produces an estimated temperature rise of < 1 °C in the sample.

Details of the Si frame fabrication, assembly of the micro-device, and procedures used for in situ electromechanical experimentation with the FEI Tecnai G2 TEM are provided in [12-14]. Sample preparation is explained in more detail in the following. Foils of single crystal copper (SCC) of 50 μm are spin-coated with photoresist layers. Then laser patterning is done with a solid-state, frequency tripled $Nd{:}YVO_4$ pulsed laser (355 nm, 10 W, repetition rate of 50 kHz, and ~90 nsec pulse width) to co-fabricate the specimen frame (5 mm x 1.5 mm) and the dog-bone shaped specimens (20-40 μm in width) from the foil. Liquid ferric chloride etching is

subsequently applied to remove the potentially laser-damaged surface material. The specimen/frame is then assembled with the other components of the micro-device, and then the nanoscale gage section (10 µm length, 100 nm x 10 µm cross-section) is produced using focused ion beam milling (FEI Nova 600) (Figure 1b-c). Lastly, the specimen frame out-riggers are then cut by either laser or mini-scissors (final test configuration shown in Figure 1a).

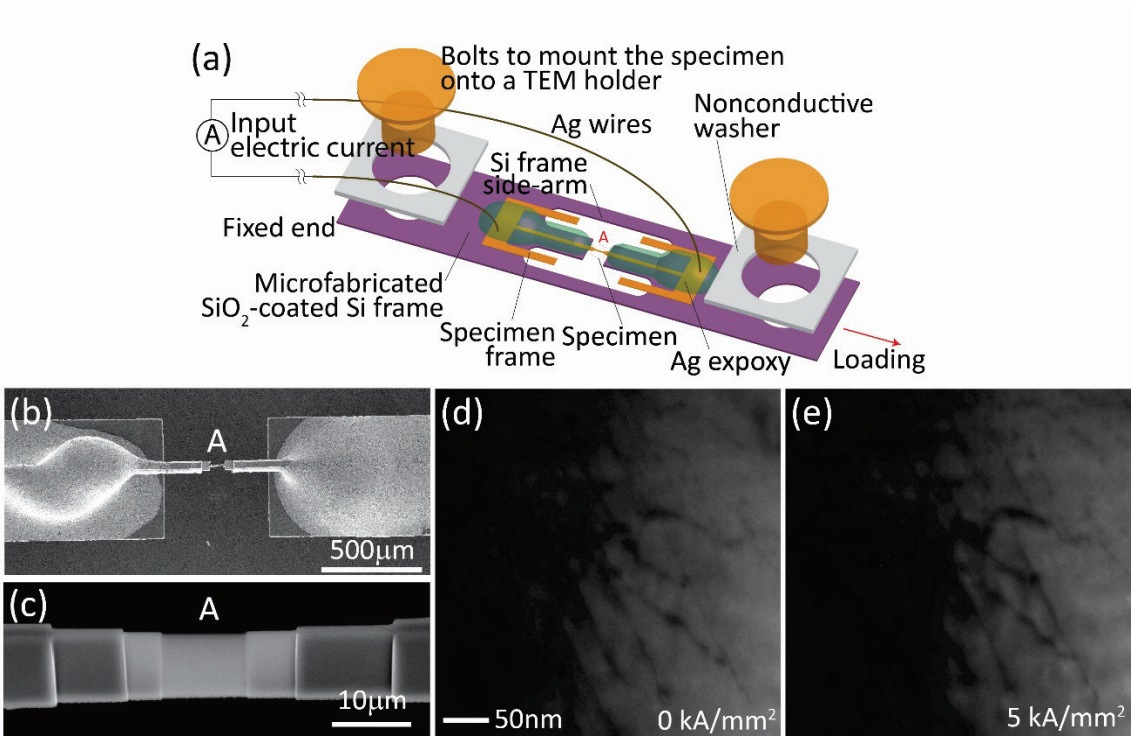

Figure 1: The novel method for *in situ* electromechanical testing of metals: (a) schematic of the NRL micro-device with major component details; (b)-(c) close-up view of the sample (A) showing the intricate design and size; and (d)-(e) static dislocations before (d) and after (e) the application of current in a mechanically strained state [12-14].

Results

The thermal drift of the specimen was quantified first to experimentally confirm the absence of significant Joule heating. Matlab-based image correlation algorithms were used to analyze TEM images at different current densities. Comparable drifts of 18.45 nm/min and 15.0 nm/min with 500 A/mm^2 and zero current density, respectively, were measured. Additionally, no change in the microstructure of the SCC specimen was found. To observe electron-dislocation interactions, the following procedure was adopted. First, tensile strain was applied incrementally using the TEM holder to the point that the observable dislocations started moving. At least one, preferably several such dislocations were placed in the field of view at that strain, and then a specific electric current density was applied. In the next step, the electric current was shut off and the smallest incremental strain was applied again. TEM images were taken at every step, a minute after the application of mechanical or electrical loading to achieve steady state. This procedure was carried out a few times on two different specimens, and the observations showed no effect of electric current on dislocation motion. For example, one case showed no movement of a

dislocation loop formed by mechanical strain under the application of 500 A/mm^2. However, the dislocation loop did move when the smallest possible strain increment was applied. This behavior was consistent up to 5 kA/mm^2 current density (e.g., Figure 1d and e).

The results showed no electron-dislocation interaction in the face-centered cubic system of SCC. However, such interactions may exist in other metals like titanium and duplex steel alloys that have a larger number of slip systems and diverse dislocation dynamics mechanisms.

Summary

In the course of this TEM study, we developed a novel micro-device method for in situ characterization of submicron-micron scale specimens under concurrent electromechanical loading in an attempt to better understand electrically-assisted deformation in metals. It provides a tool for studying electroplasticity under high current densities without large Joule temperature increases at the scale of expected electron-dislocation interactions. As a result, any observed changes from pure mechanical behavior must be attributable to the electric current. The absence of large temperature increases due to Joule heating remains in effect for large current densities (at least until 5 kA/mm^2), and the uniform cross-section of the TEM specimen permits a straightforward interpretation of the results.

The utility of the micro-device for the TEM EAD experiments was demonstrated for pure single-crystal Cu. While an electroplasticity effect was not observed with this material, a roadmap for the study of other material systems was identified.

Note that in situ electromechanical TEM experiments were planned for several other metals, but they could not be performed due to closure of the NRL Nanoscience Institute (NSI) cleanroom from March 2017 through September 2018 due to accidental flooding. The cleanroom had several pieces of equipment that were needed for making the Si micro-devices and test specimens, and these were not available for use during the closure.

CHAPTER 3: MESO-SCALE CHARACTERIZATION

Characterization of electrically-assisted deformation (EAD) in metals in prior research has produced a wide range of often contradictory findings depending on the experimental method used, which has led to confusion on the potential mechanisms for enhanced deformation under applied current. A wide range of results have been shown for AC, DC, pulsed, and constant applied currents and for tension versus compression loading. For example, Roth et al. [15] found that pulsing current during tensile testing of Al 5754 sheet metal can increase the elongation to failure, however there is an optimal period and duration of pulsing. If the pulse is too frequent or too long, the specimen can neck prematurely. Jones et al. [16] found that pulsed currents enhanced deformations during compressive testing whereas constant currents enhanced elongation during tensile testing. While it was not a focus of these prior studies, it is also expected that the physical properties of the material being tested (e.g., resistivity, dislocation density, grain size) may influence deformation enhancements with applied current.

In this research, meso-scale EAD was characterized using a custom test system that effectively decouples electrical current effects from the Joule heating to enable independent assessments of the effects of mechanical deformation, electrical current, and Joule heating on the plastic deformation behavior. The following sections and Appendix B outline the technical challenges, methods, and results in our investigation of the effects of constant electric current on the tensile plastic deformation of pure metals at the meso-scale.

Experimental challenges

Tensile experimentation with large electrical currents flowing through the specimen is first and foremost a safety challenge. Currents must be introduced into the specimen, safe operation must be guaranteed, and sensitive components and instrumentation must be isolated from the current. Experimental design required consideration of the following:

1. Load-frame modifications to enable safe passage of potentially large electric currents through the test specimen;
2. Specimen grip fixturing and hardware to achieve uniform strain, current density, and temperature conditions in the gage section;
3. Safe and accurate strain and temperature measurements along the gage length using non-contact methods, and time-synchronization and acquisition of signals from many different measurement sources;
4. Effective dissipation of the Joule heat generated by large (constant) current densities;
5. Independent experiments to decouple current density, j, and temperature, T, effects under controlled and identical field conditions.

Test Systems Description

The meso-scale experiments utilized two test systems (Figure 2). The first was a system for in situ SEM testing: SEMTester 2000 EBSD (MTI Instruments, Inc., Albany, NY). This device was

modified to enable safe passage of electric currents through the mechanical test specimen. Details of the modifications and custom hardware are provided in Appendix B. The second was a laboratory materials test system with an environmental chamber: ElectroPuls 3000 with Series 3119-405 Environmental Chamber (Instron Corp., Norwood, MA). This latter system was used to perform tensile tests with the same temperature-time profile as the applied current tests so that Joule heating could be decoupled from possible electroplasticity effects.

Meso-Scale Testing with Electric Current

The electromechanical testing facility for meso-scale specimens consisted of six primary components: screw-drive load frame, electric current supply, IR temperature measurements, video strain measurements, auxiliary thermocouple temperature monitoring, and forced-air cooling of the specimens. The schematic in Figure 3 shows the SEMTester load frame connected with the MTI Controller that is coupled with MTest Quattro software on a dedicated computer. The software enabled materials testing at a desired displacement/load-versus-time profile. Analog load and crosshead displacement output signals from the MTI controller were recorded using a National Instruments (NI) PXIe DAQ analog-to-digital converter controlled by LabVIEW software on another dedicated computer. The NI DAQ/LabVIEW system performed instrument control and collection, storage, and time synchronization between multiple independent measurement signals.

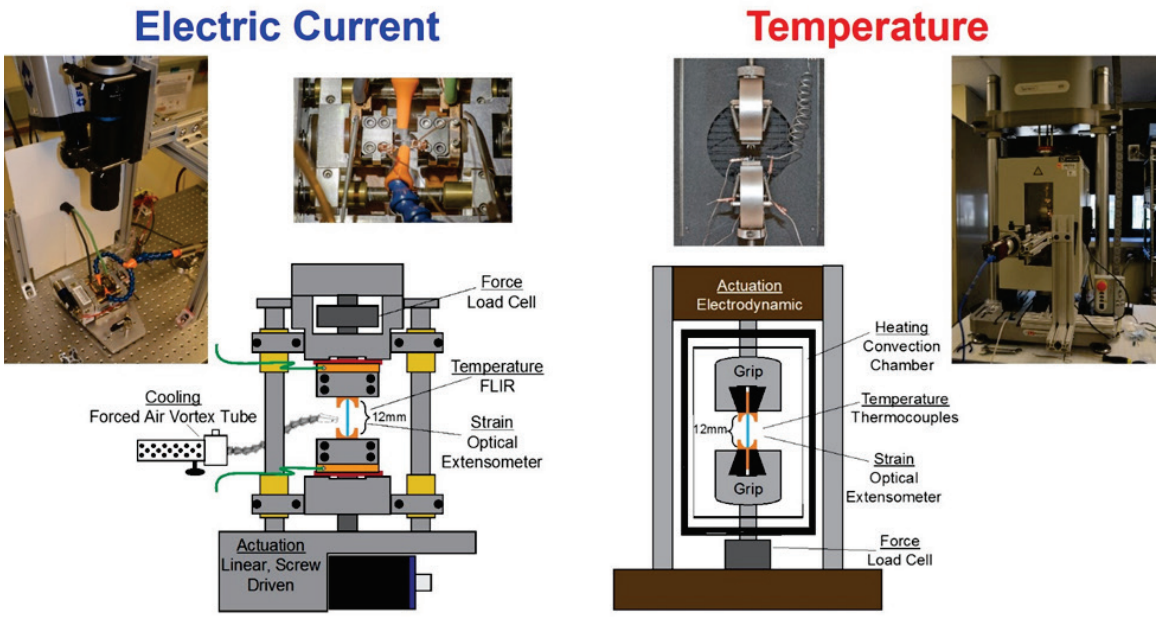

Figure 2: NRL approach for assessing electric current effects on the plastic deformation of metals at the meso-scale**.**

A power supply (Model 6690, Agilent Technologies, Santa Clara, CA) controlled by LabVIEW provided constant current (density) to the specimens and current and voltage analog outputs that are recorded by the NI DAQ/LabVIEW system during testing. A FLIR IR camera system controlled by a dedicated computer was used for full-field temperature measurements along the

specimen gage length. LabVIEW provided a trigger for the start of the IR video recording at the test start. A non-contact video extensometer system (MTS AVX) was used for measuring strains along the specimen gage length. The AVX video camera was controlled by a dedicated laptop running MTS Video Extensometer software. It stored video captured during testing and provided four real-time analog outputs (three strains and time) that were read by the NI DAQ/LabVIEW system. The AVX analog outputs were +/- 10V signals with signal-to-voltage calibration factors set in software. Several thermocouples (TC) were used to monitor temperatures at the current connections and grip fixtures for safety purposes. An adjustable spot cooler with vortex expansion-cooling of compressed air was used to provide convective cooling of the Joule heat and minimize increases in specimen temperature and gradients along the gage length.

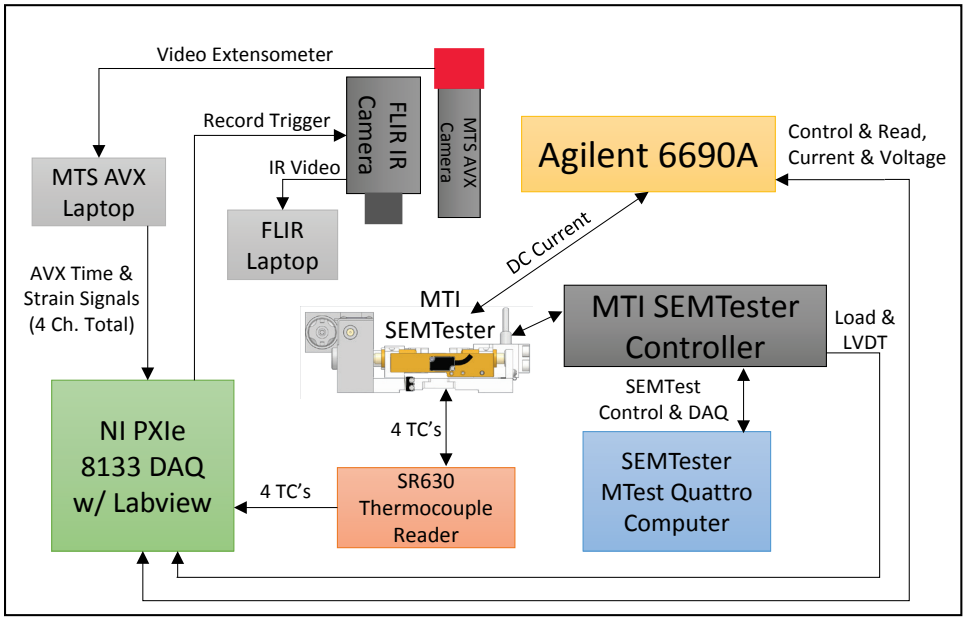

Figure 3: Data flow diagram for the equipment and software controlling the MTI SEMTester experiment.

Meso-Scale Testing without Electric Current

The setup for running the complimentary temperature experiments without electric current consisted of four main components: load frame, environmental chamber, thermocouple reader, and AVX non-contact strain measurement system. The Instron load frame and environmental chamber were controlled by a dedicated computer running Bluehill software. The load from the Instron was output as an analog signal that was read by the NI DAQ/Labview system. Temperature was measured by thermocouples attached at the specimen tabs, grips, and on a length of wire of same material being tested adjacent to the specimen for accurate temperature readings independent of thermal conductivity mismatch. The AVX strain system provided four analog outputs (three strains and time) that were read by the NI DAQ/Labview system. The front door of the environmental chamber included a window to permit visual strain measurements. The NI DAQ/Labview system provided time-synchronization and recording of the various data streams in a single file for post-processing.

Temperature and Strain Measurement Details

Accurate temperature measurements using IR required a surface thermal emissivity equal to ~1. A sprayed-on graphite coating (GRAPHIT 33, Kontakt Chemie/CRC Industries Group) was used for this purpose. The graphite coating adhered well, in general, but tended to debond at spots on the specimen surface at large plastic strains (e.g., after necking). The FLIR IR camera (SC8300HD, FLIR Systems) was controlled by ResearchIR software (FLIR Systems). The camera used a 100 mm lens and was run at a frame rate of 15 Hz. Minimum and maximum temperatures (between -20 and 350°C, ± 2°C resolution) and specific measurement points on the specimen gage section were setup in the software prior to running the test, and digitally recorded video allowed for post-test analyses of the specimen temperatures and gradients.

Thermocouples were attached to small Cu alligator clips for monitoring load frame component temperatures (e.g., electrical leads, grips, and load cell) to avoid possible thermal damage with the passage of high test currents. The thermocouples were hardwired to a Stanford Research SR630 conditioner that provided analog outputs to the NI DAQ/LabVIEW system. The SR630 electrically isolated the signals to avoid possible grounding that would have permitted large current flows from the specimen to the SR630 and NI DAQ/LabVIEW systems. Inadvertent grounding of the specimen would have been a significant safety issue.

The AVX video extensometer (Part No. 574281-04, MTS Systems Corporation, Eden Prairie, MN) was used for specimen strain measurements. The system employed a camera (Model Manta G146B ASG, Allied Vision Technologies) with attached lens (Sill Optics Correctal T/0,2D) with an f-stop setting of 11 and video capture frame rate of 5 Hz. The video extensometer could track the motion of up to 100 points in real time. The displacement measurements used a scaling factor of ~ 43 pixels/mm (23 μm/pixel). Strains, displacements, rotations, etc. could be calculated as desired from the stored video data post-test. To generate marks for video strain tracking, a high-temperature white paint was speckle patterned onto the specimens using an air brush at low pressure (~0.035 MPa (~5 psi)) with a steady even stroke. Non-contact strain measurement enabled accurate strain data irrespective of potential slipping in the grips, grip-to-gage geometry transitions, and machine compliance effects.

Forced-Air Cooling Details

The Instron environmental chamber used for baseline temperature effect tests is limited to a maximum of 250°C. This was adopted as the maximum allowable temperature during electromechanical testing, which was controlled by the applied test current density, the specimen material resistivity, and the effectiveness of the forced-air cooling system. Earlier attempts at specimen cooling were not effective enough in extracting heat from the specimens (see Appendix B). Specimen cooling capability limits the maximum current densities that can be used in testing, particularly with higher resistivity materials like Ti and Fe. A new approach using a vortex air cooling device was developed. A Frigid-X adjustable spot cooler (NueAir Engineered Products, Cincinnati, OH) that uses compressed air was adopted. The 710 L/min (25 SCFM) brass vortex generator with an input pressure of ~0.5 MPa (70 psi) produced ~500 L/min (17.5

SCFM) flow through the cooler (Figure 4) and 360 W of cooling. The chilled air was split to flow through two nozzles aimed at two sides of the specimen (Figure 5), which was effective in minimizing overall specimen temperature and gradients along the gage length. The chilled convective air enabled maximum current densities of 200, 70, and 45 A/mm^2 and corresponding maximum temperatures at peak loading of 112, 134, and 222°C for copper, iron, and titanium, respectively.

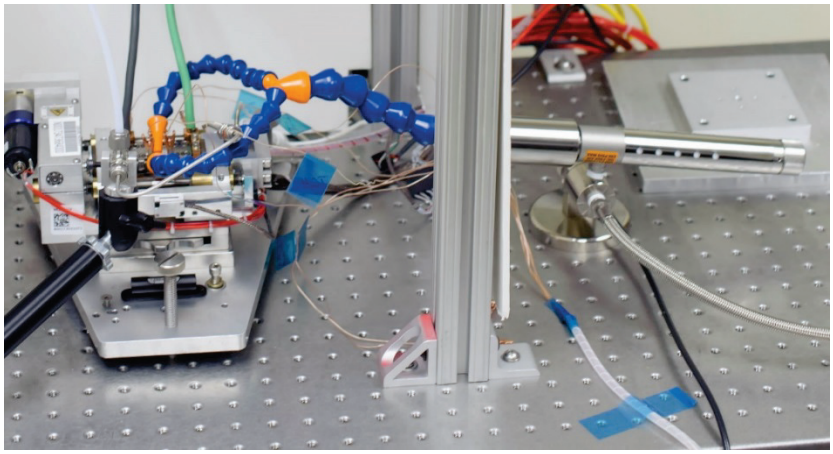

Figure 4: Frigid-X adjustable spot cooler for convective air cooling of the specimens during electric current testing.

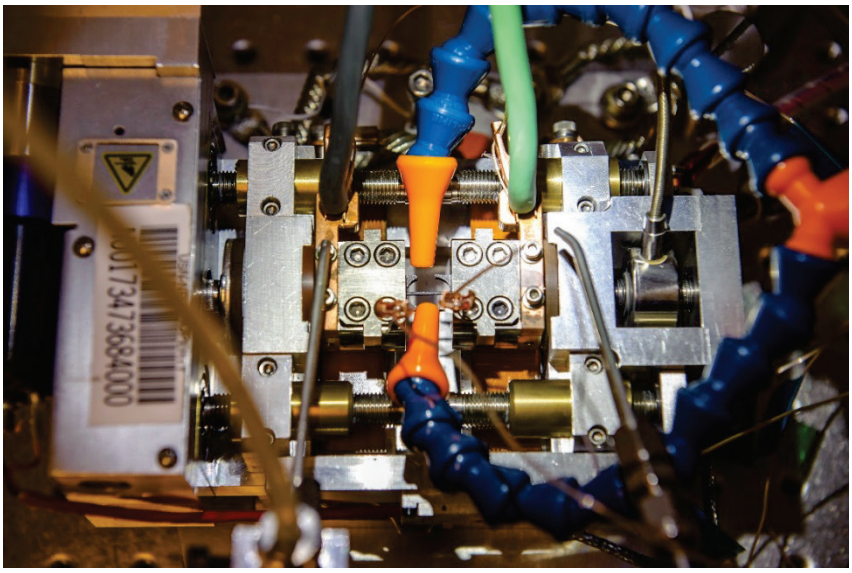

Figure 5: Meso-scale load-frame showing a wire tensile specimen being cooled by chilled air through two orange spreader-nozzles. The two stainless steel tubes provide a N_2 flow for cooling the current-grip connections.

This novel cooling system combined with the specimen geometry and tab-gripping (described below) effectively transferred heat from the test specimen for limiting the maximum temperature and for minimizing temperature gradients along the gage length (Figure 6a). Other cooling methods (and specimen designs) described in Appendix B or reported in the literature (e.g., Figure 6b) have not shown the same heat transfer/temperature control capabilities.

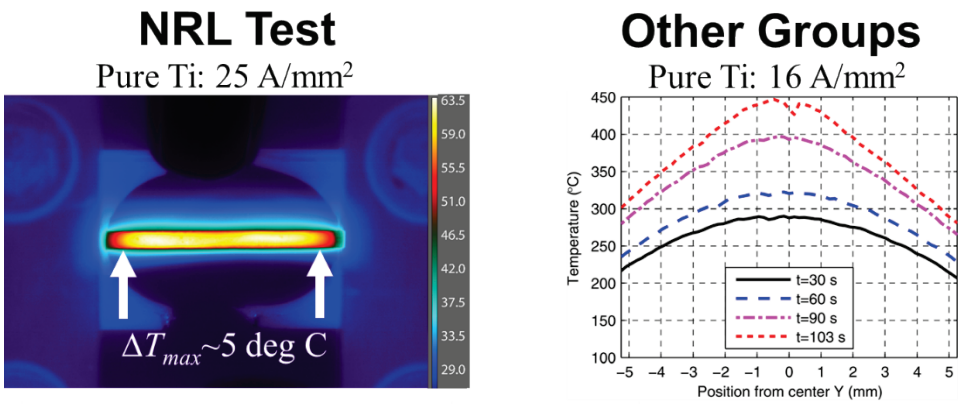

Rudolf et al., in preparation, 2018 *Magargee et al., 2013*

Figure 6: Comparison of gage-section temperature gradients between (a) the NRL test setup and (b) tests performed by Magargee et al. [17].

Materials and Specimen Preparation

High-purity metal (wire) samples of Cu, Fe, and Ti were selected for testing. Suppliers and purities are listed in Table 1, and nominal properties are listed in Table 2.

Table 1: Material suppliers and purities. Supplied as 1 mm diameter (nominal) wires.

Material	Crystal Structure	Vendor	Purity	Temper
Copper (110 ETP)	Face-centered cubic	McMaster Carr	99.9%	Annealed
Iron	Body-centered cubic	Goodfellow Corp.	99.99%	As Drawn
Titanium (CP Grade 2)	Hexagonal close-packed	Goodfellow Corp.	99.99%	As Drawn

Table 2: Nominal material properties[a].

Material	**Density (g/cm^3)**	**Specific Heat (J/kg-°C)**	**Resistivity (nΩm)**	**Melting Temperature (°C)**	**Yield Strength (MPa)**	**Tensile Strength (MPa)**	**Modulus (GPa)**
Cu (110 ETP)	8.96	385	16.9	1083	54 - 270	240	117.0
Fe	7.78	444	101	1535	120 – 150	180 – 210	211.4
Ti (CP Grade 2)	4.50	523	540	1660	140 - 250	230 - 460	120.2

[a] from "Material Properties" at the Goodfellow.com website: (http://www.goodfellow.com/catalogue/GFCat2.php?ewd_token=rKlE9uKiEE5Wze2uFpUoOHFDzPQjlS&n=imauPXj58Szjrv6KvR7O2UMgPLdP2A). Last accessed on: 24-Sep-2018.

Circular-wire specimens were adopted for meso-scale testing as described in Appendix B. The selected 1.0 mm nominal diameter was a compromise that balanced the amount of Joule heat generation/cooling and the failure load levels (load cell limitations). Aluminum tabs were designed and fabricated for supporting the wire test samples with a nominal 12 mm gage length in the SEMTester. The tabs distributed the wedge-grip clamping forces so that specimen failure would occur in the gage section and not the grips. They provided good metal-metal contact between the grip, tab, and wire for getting electric current into the specimen without hot-spots

and for providing good thermal conduction paths for extracting heat generated in the gage section. The tabs included "outriggers" for handling stability and alignment during mounting; they were cut after clamping in the SEMTester wedge grips just prior to testing. See Appendix B for more details on specimen sizing, tabs, and cooling.

The wire materials were supplied in wound-coil forms. The drawing and winding processes created significant residual stresses. Manually straightening the wires for testing required large plastic deformations, so a stress-relief process was developed to straighten the wires and relieve the residual stresses. Fixturing was made for stress-relieving four lengths of wire at a time. It consisted of two bars ~290 mm in length made from the same materials (e.g. Cu bar for the Cu wire). Each bar had four 1 mm diameter half-circle channels for holding the wires straight by sandwiching during stress-relief. The fixtures are shown in Figure 7, and a machining print can be found in Appendix B (Figure 36). Up to four wires could be clamped between the two bars, bolted together, then oven heated in ambient air at the temperatures and times listed in Table 3.

Figure 7: Stress-relief fixtures for straightening the wire samples. (Top and middle) inside view of the Ti, Cu, and Fe fixtures showing four "wire-tracks"; and (bottom) exterior view of the Ti fixture clamped and bolted.

Table 3: Stress-relief parameters and grain sizes[b].

Material	Temperature (°C)	Time (hours)	Grain Size (μm)
Copper (110)	190	2	3.3
Iron	425	2	5 & 10 bi-modal
Titanium (CP Grade 2)	500	2	9

[b]: Grain sizes of the as-received and stress-relieved specimens were identical.

The stress-relief treatments produced straight wires with no residual stresses. Subsequent metallurgical examinations showed that they had no effect on the "as-received" microstructures (grain sizes). The straightened wire specimens provided a common (residual stress-free) baseline

for the originally coiled as-received materials. Straight wire specimens were also much easier to assemble (sandwiching between tabs, graphite and white speckle painting), mount, and align in the SEMTester and Instron wedge grips.

Test Procedures

Specific tests for each material (Cu, Fe, and Ti) consisted of zero-current baseline runs on each system (SEMTester and Instron), non-zero current runs at two current density levels with the SEMTester system, and temperature-history matched runs at zero-current on the Instron system. All experiments were performed using cross-head displacement control with an extension rate of 0.15 mm/min until break.

Non-Zero Current Testing: SEMTester

Some preliminary tests for each material type were conducted with operative specimens and specimen-fixture cooling to determine the current density levels that would produce gage-section temperatures greater than 200°C or grip temperatures greater than 50°C. This defined the larger (maximum) test current for each material. Current densities below these maximums would not produce gage temperatures above 250°C, the limit for the Instron environmental chamber, nor pose a risk to the SEMTester (load cell, etc.). The lower current density test level was selected to be roughly 2/3 of the maximum. Replicate tests (two or three) were performed for each material, at each current density (SEMTester: zero, low, and max) and at each temperature (Intron: baseline, intermediate, and high) for assessing variability in the results. The results tabulated in Tables 4-6 show how many replicate tests were performed at each condition.

Zero Current Testing: Instron

Specimens for each material were tested at room temperature with zero-current on both the SEMTester and Instron systems a for side-by-side comparisons of baseline stress-strain responses (which were identical, as expected). Specimens were first tested with the SEMTester at the desired current levels. The resulting thermal histories (averaged gage temperature versus time) were programmed in the Instron environmental chamber for creating the same temperature history in the zero-current, chamber-heated specimen tests. Precisely matching the current-induced temperature histories in the zero-current temperature tests provides the most accurate baseline for differentiating current and temperature effects on the plastic deformation response.

Figure 8 shows temperature profiles for the high current density tests on the three pure metal specimens. It shows increases in temperature with time and a sharp increase after reaching the ultimate load where the cross-section reduces. Typical temperature increases prior to necking were: Cu → 25°C; Fe → 50°C; and Ti → 150°C. The more rapid temperature increases after necking could not be followed by the environmental chamber leading to some discrepancies towards the test ends. The reduction in cross-section area with necking is highly localized, and it

produces large increases in current density (Joule heating) and temperature at the neck. Gage-averaging of the temperature after necking has occurred is not appropriate.

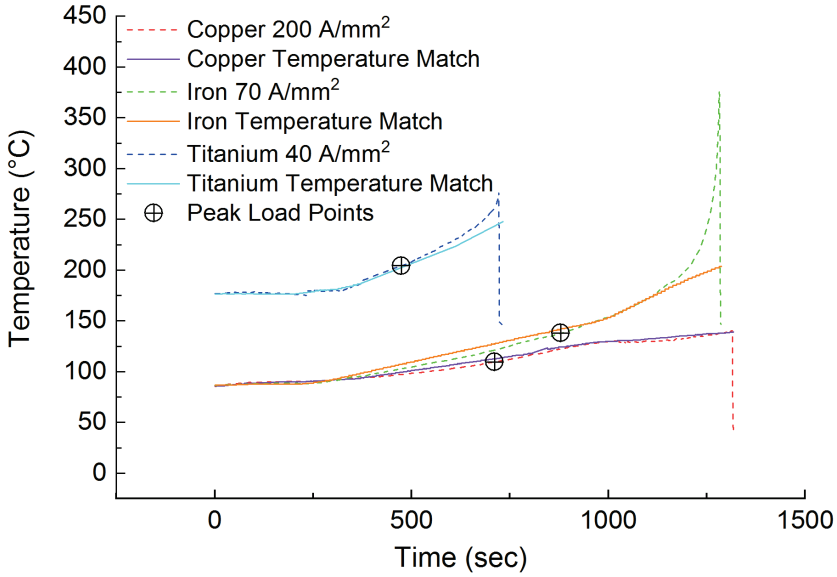

Figure 8: Gage-section (averaged-dashed lines) thermal histories from the electric current tests and the matching (averaged-solid lines) thermal histories from the zero-current tests.

Some procedures reported in the literature [1, 10] have used a single average or maximum temperature from the applied current test for the temperature control point in the matching zero-current test. A constant temperature does not accurately represent the temperature-time and temperature-location responses in the applied current test specimens, particularly in the presence of large temperature gradients and/or necking deformations.

Results

The tensile response data for replicate tests (identical current, temperature-time, displacement rate conditions) showed good consistency. Variations in ultimate strength were below 1.4% for the Cu and Fe samples and 2.7% and 5.8% for Ti samples at the low and high current densities, respectively. Averaged stress-strain curves are calculated for each material and test condition for assessing the effects of electric current and temperature on the tensile deformation responses.

Copper

The copper wire specimens were tested with constant direct current densities of: 0, 125, and 200 A/mm^2. The average grain size was 3.3 μm before and after stress-relief treatment, and no changes in grain size were observed after testing (all conditions). The maximum temperature reached during applied current testing was ~113°C at 200 A/mm^2, and this is below the stress-relief temperature.

Increasing reductions in the flow stresses, ultimate strengths, and strains at maximum load occurred with applied current and matched temperatures (Table 4, Figure 9), but no differences were observed in the flow stresses and ultimate strengths between the applied current and

matching temperature tests. Failure strains (elongations) were significantly reduced in the applied current tests, as a consequence of the increased current density at the neck, which raises the temperature and reduces the strength. No such changes were observed in the matched temperature tests. The fracture area in the neck of the applied current specimens was much smaller than that of the matched temperature specimens. Yield strengths were reduced similarly by current and temperature. Electric current has no apparent independent effect on the stable (pre-necking) plastic deformation behavior of this pure Cu material.

Table 4: Test results for the pure copper (99.9%, annealed) samples.

Sample	Current Density (A/mm^2)	Area (mm^2)	Temperature (at peak load) (°C)	Temperature Gradient (at peak load) (°C)	Peak Load (N)	Ultimate Strength (MPa)	Axial Strain (at peak load) (% extension)	Yield Strength (0.2 % offset)	Young's Modulus (GPa)
Cu - l	RT	0.8155	RT - 23.7	N/A	195.8	240.1	20.72	201.5	118.6
Cu - m	RT	0.8155	RT - 23.4	N/A	197.3	241.9	21.65	204.2	120.2
Cu - o	RT	0.8171	RT - 21.7	N/A	193.8	237.2	22.87	194.8	119.9
Cu - c	125	0.8198	63.7	5.7 [58.0-63.7]	173.9	212.1	16.04	190.2	120.2
Cu - i	temp. profile to match c	0.8198	N/A	N/A	179.0	218.4	15.59	189.7	114.7
Cu - f	125	0.8139	70.0	7.3 [62.7-70.0]	177.4	217.9	16.92	197.0	119.7
Cu - j	temp. profile to match f	0.8187	N/A	N/A	178.6	218.2	15.88	192.6	113.7
Cu - g	200	0.8155	109.7	9.8 [99.9-109.7]	157.2	192.7	8.12	181.1	113.2
Cu - k	temp. profile to match g	0.8219	N/A	N/A	156.7	190.6	7.55	180.7	117.2
Cu - h	200	0.8155	113.0	9.6 [103.4-113.0]	155.7	190.9	9.86	179.5	118.3
Cu - n	temp. profile to match h	0.8171	N/A	N/A	158.4	193.9	7.35	178.9	118.2

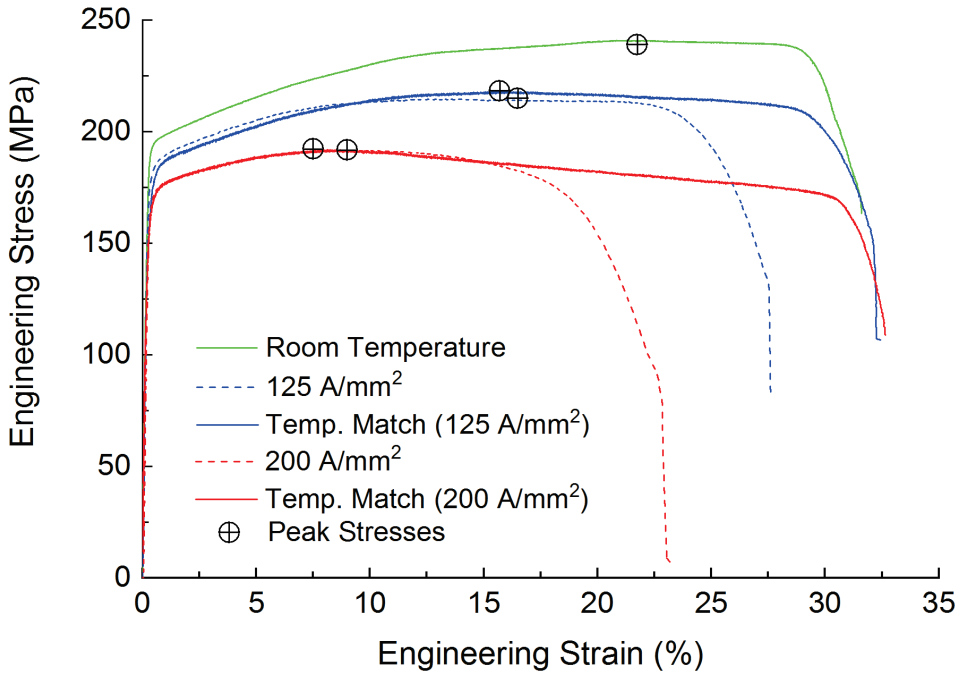

Figure 9: Stress-strain curves for the copper specimens. The curves are averages at each condition, and the ultimate strengths (onset of necking) are marked with the crossed-circle. All experiments were performed in cross-head displacement control with an extension rate of 0.15 mm/min until break.

These results differ from Jiang et al. [18] who found that electric current reduced the tensile flow stress by ~10% more than tests at the matched temperature. Their experiments utilized short dc current pulses and a faster displacement rate of 1 mm/min. Experiments with Cu (C11000 alloy) by Ross et al. [19] utilized constant direct current densities up to 73.9 A/mm^2 and found decreases in the yield strength and elastic modulus with increased current. Flow stress reductions with increasing current densities were noted, but matching thermal tests were not performed to identify the separate contributions from Joule heating. Some EAD results reported in the literature [1, 18, 19] saw no effects of current on the failure elongation values.

Iron

Iron wire specimens were tested under constant, direct current densities of: 0, 45, and 70 A/mm^2. There was a bi-modal grain size distribution with 5 and 10 μm averages before and after stress-relief treatment and after testing (all conditions). The maximum temperature during testing was ~140°C at the 70 A/mm^2 current density, which is below the stress-relief temperature.

Reductions were observed in the flow stress, ultimate strength, and strains at maximum load with both applied current and elevated temperature conditions (Table 5, Figure 10). Failure strains were significantly reduced with applied current, and to a lesser degree with elevated temperature. Reductions in strain at failure with temperature only did not occur with the Cu. Yield strength was reduced by the applied current and the temperature at the higher level (e.g., 70 A/mm^2), but it appeared to increase slightly at the intermediate current/temperature levels (e.g., 45 A/mm^2). Temperature was more effective in reducing Young's modulus than applied current. In conclusion, electric current does not independently affect the stable (pre-necking) plastic deformation behavior of this pure Fe material.

Table 5: Test results for pure iron (99.99%, as-drawn) samples.

Sample	Current Density (A/mm^2)	Area (mm^2)	Temperature (at peak load) (°C)	Temperature Gradient (at peak load) (°C)	Peak Load (N)	Ultimate Strength (MPa)	Axial Strain (at peak load) (% extension)	Yield Strength (0.2 % offset)	Young's Modulus (GPa)
Pure Fe - 5	0 - RT	0.7922	N/A	RT - 21.2	256.6	323.9	20.53	257.2	200.3
Pure Fe - 6	45	0.7943	55.6	5.8 [49.8-55.6]	246.4	310.2	13.72	268.2	193.0
Pure Fe - 10	temp. profile to match 6	0.7933	N/A	N/A	244.2	307.8	15.86	259.7	187.0
Pure Fe - 8	45	0.7943	52.1	7.2 [44.9-52.1]	248.7	313.1	11.48	276.4	194.3
Pure Fe - 13	temp. profile to match 8	0.7943	N/A	N/A	248.1	312.4	14.21	271.0	185.2
Pure Fe - 7	70	0.7933	132.6	8.8 [123.8-132.6]	220.0	277.3	7.72	256.0	185.7
Pure Fe - 11	temp. profile to match 7	0.7959	N/A	N/A	220.1	276.6	7.20	253.2	180.6
Pure Fe - 9	70	0.7906	140.0	5.5 [134.5-140.0]	216.6	274.0	10.94	242.3	193.5
Pure Fe - 12	temp. profile to match 9	0.7959	N/A	N/A	221.2	277.9	9.53	246.7	179.7

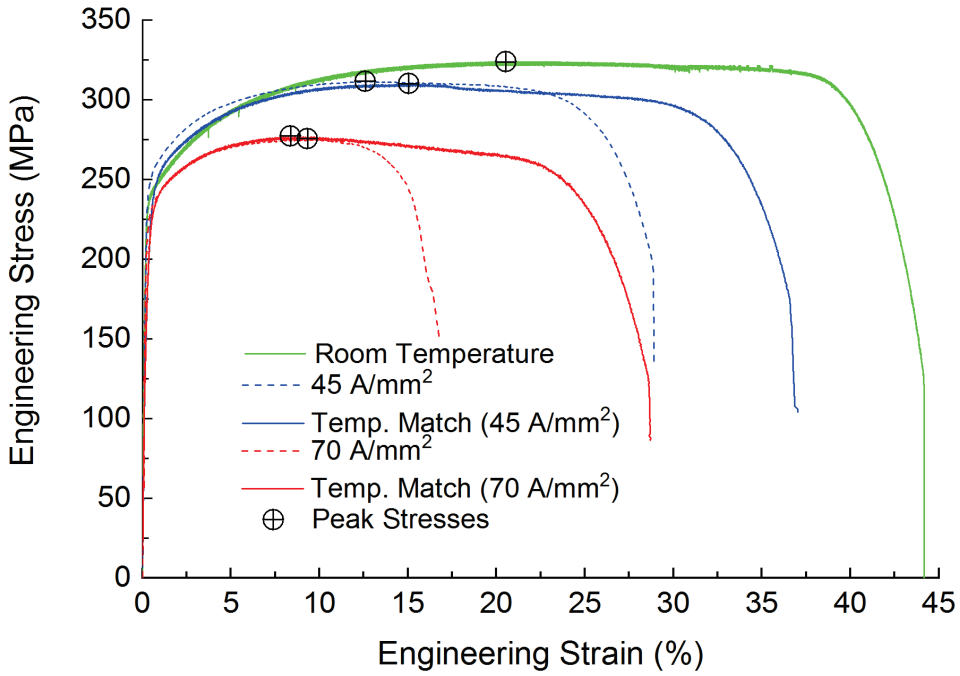

Figure 10: Stress-strain curves for the iron specimens. The curves are averages at each condition, and the ultimate strengths (onset of necking) are marked with the crossed-circle. All experiments were performed in cross-head displacement control with an extension rate of 0.15 mm/min until break.

Titanium

Titanium wire specimens were tested under constant, direct current densities of: 0, 25, and 40 A/mm^2. The average grain size was ~9 μm before and after stress-relief treatment, but in this case, significant changes in the grain size were observed after testing at the two applied currents but not at the corresponding temperature matched conditions.

Similar to the Cu and Fe results, reductions were observed in the flow stress, ultimate strength, and strains at maximum load with both applied current and elevated temperature (

Table 6, Figure 11). *However, the ultimate strengths were reduced by an additional 19 and 22% with the applied current versus the reductions occurring with matching temperature conditions.* Failure strains were significantly reduced by the current relative to matched temperature values. The final failure part of the stress-strain curve for the room temperature Ti specimens is not available; for the two curves used in the average, one specimen failed at the tab-gage interface and the other lost the surface strain markings prior to fracture. Electric current was more effective in reducing yield strength than temperature, and both applied current and temperature caused a slight decline in Young's modulus. Electric current has a distinct (from temperature) and significant effect on the stable (pre-necking) plastic deformation behavior of this pure Ti material.

Post-test examination of the microstructure showed increases in grain size occurred in the specimens subjected to applied current (Figure 12 b,d). The observed grain growth occurred primarily in the interior with little or no change in size or shape at/near the wire surface (within

50 to 75 μm). Grain growth occurred at all points along the gage length, not just in the necking region (see APPENDIX A). No changes in grain size were observed in the companion matched temperature tests nor during the stress-relief treatment. Figure 13 shows the Ti temperature responses at the higher (40 A/mm^2) and lower (25 A/mm^2) currents. The maximum surface temperatures were below 280°C and 90°C respectively, well below the 500°C stress-relief temperature that showed no grain growth.

Table 6: Test results for the pure titanium (99.99%, as-drawn) samples.

Sample	Current Density (A/mm^2)	Area (mm^2)	Temperature (at peak load) (°C)	Temperature Gradient (at peak load) (°C)	Peak Load (N)	Ultimate Strength (MPa)	Axial Strain (at peak load) (% extension)	Yield Strength (0.2 % offset)	Young's Modulus (GPa)
Pure Ti - I4	RT	0.7854	RT - 22.0	N/A	240.5	306.1	18.82	281.5	118.6
Pure Ti - I3	RT	0.7854	RT - 23.8	N/A	237.4	302.3	18.07	277.6	109.1
Pure Ti - 9	25	0.7833	63.2	4.1	180.8	230.8	8.80	218.7	97.7
Pure Ti - I5	temp. profile to match 9	0.7870	N/A	N/A	223.7	284.2	13.12	270.3	102.7
Pure Ti - 5	25	0.7869	74.8	5.8	172.3	218.9	8.95	209.9	100.0
Pure Ti - 12	temp. profile to match 5	0.7885	N/A	N/A	213.5	270.7	13.11	259.7	102.8
Pure Ti - 6	40	0.7885	234.1	9.8	112.7	142.9	3.65	141.7	93.6
Pure Ti - 11	temp. profile to match 6	0.7869	N/A	N/A	147.9	188.0	10.38	183.4	96.0
Pure Ti - 10	40	0.7896	208	9.7	126.7	160.5	2.75	159.1	101.1
Pure Ti - I10	temp. profile to match 10	0.7880	N/A	N/A	157.8	200.2	5.37	193.8	93.0

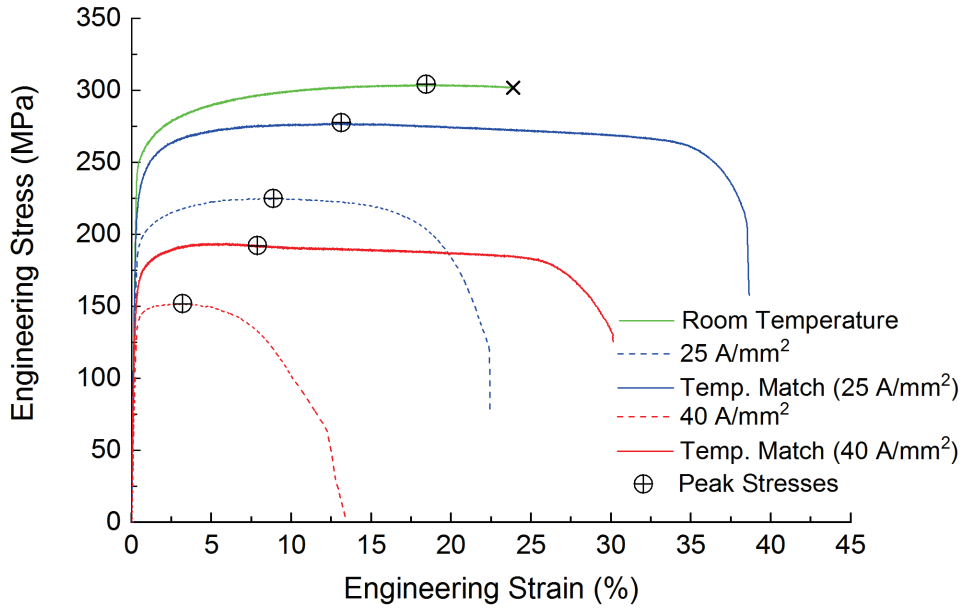

Figure 11: Stress-strain curves for the titanium specimens. The curves are averages at each condition, and the ultimate strengths (onset of necking) are marked with the crossed-circle. All experiments were performed in cross-head displacement control with an extension rate of 0.15 mm/min until break. The room temperature specimens had recurring testing problems at large strains close to failure, which render the stress-strain data unreliable.

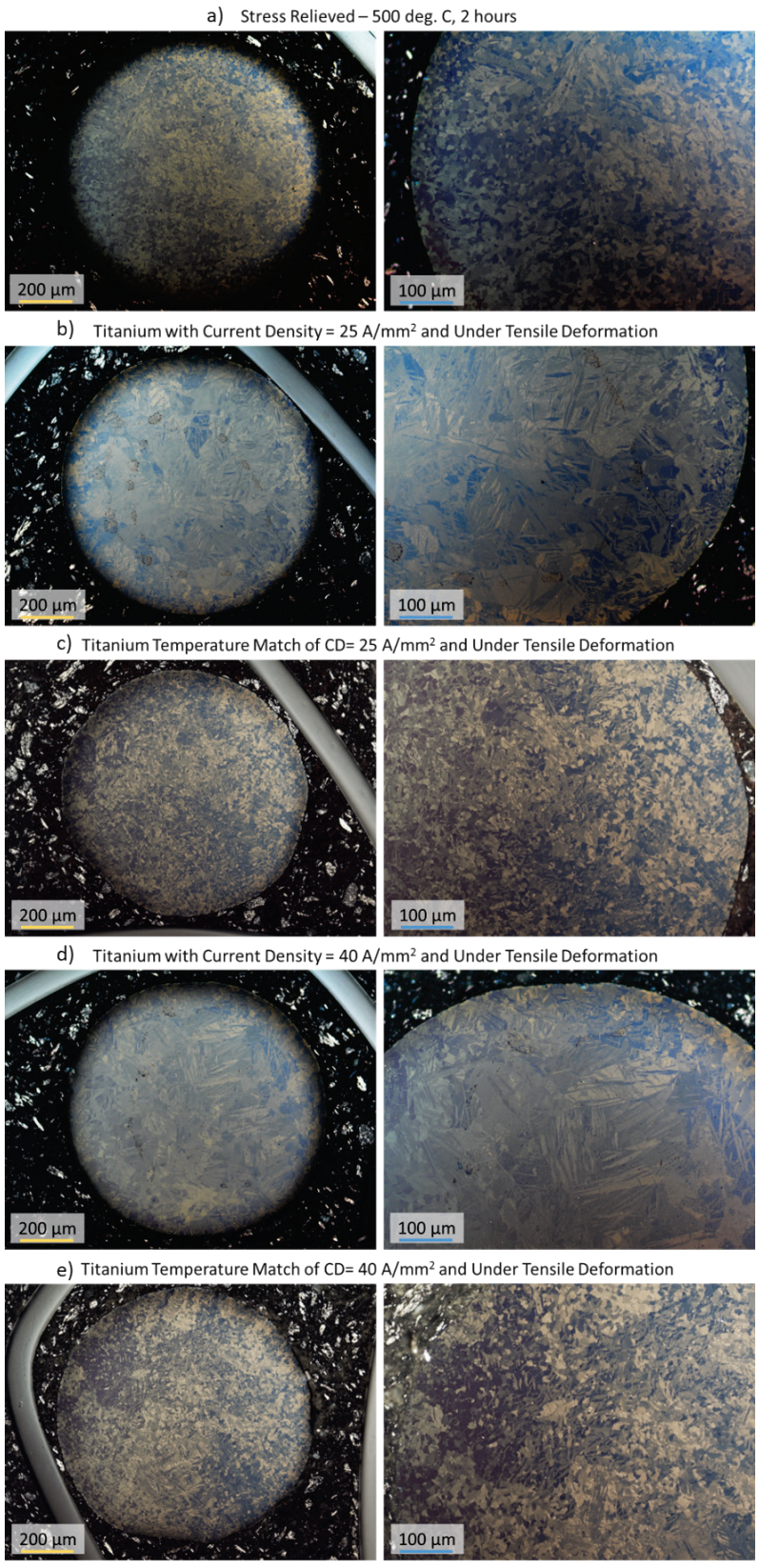

Figure 12: Cross-section micrographs for the titanium ~3 mm from the neck using cross-polarization illumination.

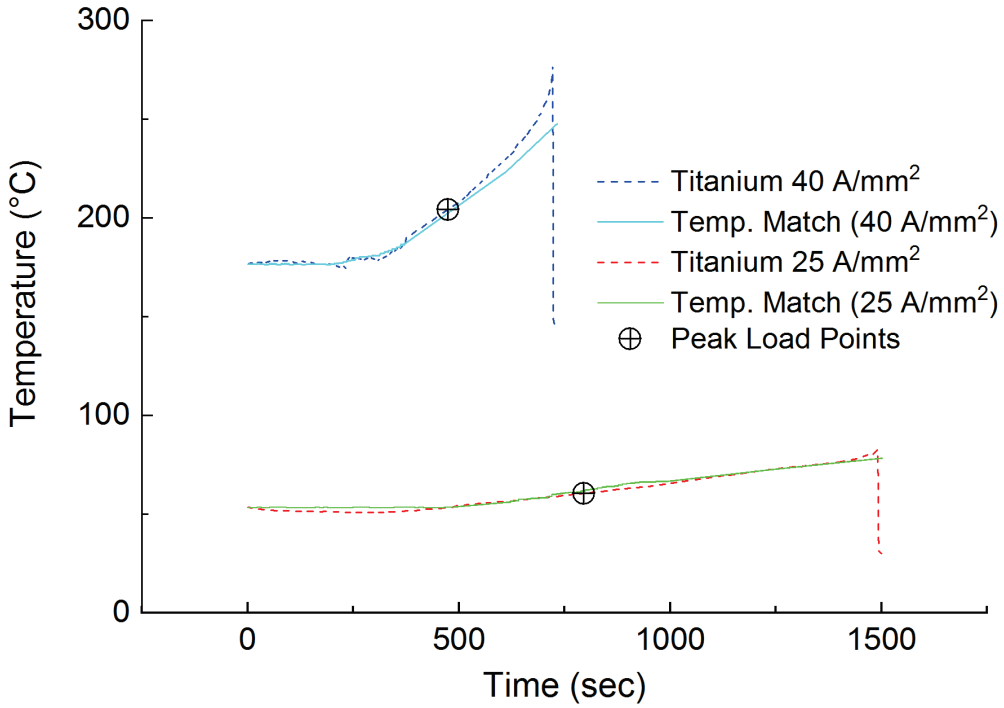

Figure 13: Temperature-time profiles for the Ti tests with current and matched temperature.

Additional experiments were performed to examine coupling effects between the electric current, temperature and mechanical deformation. Wire tensile specimens were placed in the SEMTester and subjected to the same current densities and cooling conditions as the earlier tests but without any mechanical loading. All the other parameters were kept similar (e.g., length of test, specimen temperature profile). Specimen micrographs for these tests (Figure 14) show no grain growth, which implies that mechanical deformations concurrent with the applied current and concomitant temperature rise are a necessary factor in the observed grain growth.

Another concern was the possibility of large temperature differences between the wire interior and surface. The temperature distribution in an infinite cylinder with volumetric (Joule) heating and surface convection (constant temperature) can be analytically solved for the difference between centerline and surface temperatures, $T_0 - T_{surf}$:

$$T_0 - T_{surf} = \frac{\dot{q} d^2}{16k}, \text{ where } \dot{q} = \frac{I^2 R}{volume} = \frac{j^2}{\sigma}$$

where d is the wire diameter, k is conductivity, j is the current density, and σ is the resistivity. For CP titanium: $k = 19 \left[\frac{W}{mK}\right]$ and $\sigma = 2.4 \times 10^6 \left[\frac{1}{\Omega m}\right]$. The model predicts the following temperature difference for $d = 0.001\ [m]$ and $j = 40 \times 10^6\ \left[\frac{A}{m^2}\right]$:

$$T_0 - T_{surf} = \left(\frac{(40 \times 10^6)^2}{2.4 \times 10^6}\right) \times \left(\frac{0.001^2}{16 \times 19}\right) = 2.2°\text{C}$$

This small predicted temperature difference between the surface and interior at 40 A/mm^2 current density suggests that thermal gradients are not a factor in the grain size inhomogeneity.

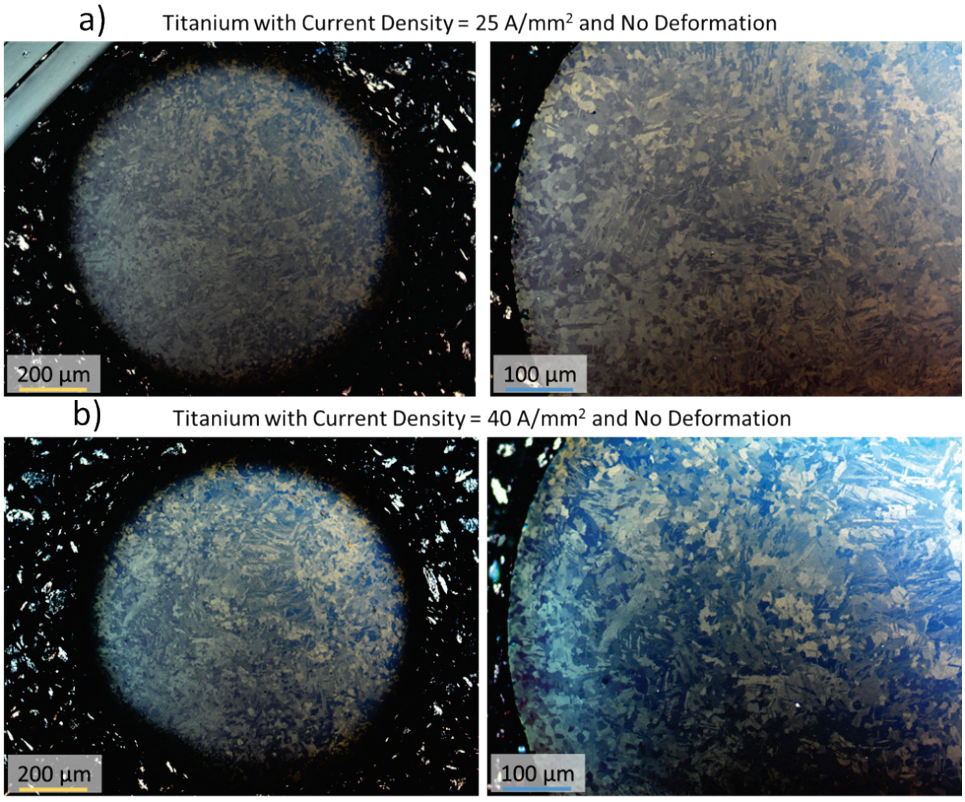

Figure 14: Microstructure images of Ti specimens after the application of electric current.

Summary and Future Work

A summary of results for the three materials and various test conditions is given in Table 7. No discernable effects of current on the plastic deformation behavior of the pure Cu and Fe materials were detected beyond those due to temperature. Current did have an appreciable effect on the flow stress and ultimate strength of the pure Ti material, showing an additional ~20% reduction beyond that due to elevated temperature. Post-test examination of the Ti microstructure showed that significant grain growth occurred during testing. Grain growth in Ti (CP Grade 2) under the combined effects of mechanical deformation, electric current, and elevated temperatures, but below the recrystallization temperature, is a new finding that has not been noted in the literature.

Analysis of the possible mechanisms for the Ti grain growth and its effect on plastic deformation is ongoing. Non-thermal (mechanical deformation) and thermal factors played a role in the observed grain growth, and the possibility of an electroplasticity role has not been ruled out. It is possible that mechanical straining drives grain growth at temperatures lower than expected. Texture evolution in the Ti grains would produce anisotropic (electrical) resistivity that might lead to localized heating. This possibility is being explored using x-ray diffraction (XRD) and electron backscatter diffraction (EBSD) analyses. The heat transfer analysis described earlier

seems to rule out the possibility of large temperature gradients within the wire specimens. Traditional grain coarsening would occur if the (wire) internal temperatures reached levels much greater than those measured on the surface, and this would lead to increases in twin density. This is being examined using EBSD. Beyond the observed grain growth, the reduction in ultimate strengths by Coble creep is being studied, which would imply grain rotation and no increases in twin density. These ongoing mechanistic analyses will be reported in the future journal publication.

Table 7: Summary of the meso-scale testing results.

Sample	Current Density (A/mm^2)	Temperature (at peak load) (°C)	Peak Load (N)	Ultimate Strength (MPa)	% Change in Strength	Axial Strain (at peak load) (% extension)	Yield Strength (0.2 % offset)	% Change in Yield Strength	Young's Modulus (GPa)	% Change in Young's Modulus
Cu	RT	22.9	195.6	239.1	-	21.75	200.2	-	119.6	-
Cu	125	66.9	175.7	215.0	↓ 1.05%	16.50	193.6	↑ 1.26%	120.0	↑ 5.08%
Cu	Temp. Match 125	-	178.8	218.3		15.70	191.2		114.2	
Cu	200	111.4	156.5	191.8	↓ 0.26%	9.00	180.3	↑ 0.28%	115.8	↓ 1.61%
Cu	Temp. Match 200	-	157.6	192.3		7.50	179.8		117.7	
Fe	RT	21.2	256.6	323.9	-	20.53	257.2	-	200.3	-
Fe	45	53.9	247.6	311.7	↑ 0.52%	12.60	272.3	↑ 2.60%	193.7	↑ 4.08%
Fe	Temp. Match 45	-	246.2	310.1		15.04	265.4		186.1	
Fe	70	136.3	218.3	275.7	↓ 0.58%	9.33	249.2	↓ 0.32%	189.6	↑ 5.22%
Fe	Temp. Match 70	-	220.7	277.3		8.37	250.0		180.2	
Ti	RT	22.9	239.0	304.2	-	18.45	279.6	-	113.8	-
Ti	25	69.0	176.6	224.9	↓ 18.96%	8.88	214.3	↓ 19.13%	98.9	↓ 3.79%
Ti	Temp. Match 25	-	218.6	277.5		13.12	265.0		102.8	
Ti	40	221.1	119.7	151.7	↓ 21.84%	3.20	150.4	↓ 20.25%	97.4	↑3.06%
Ti	Temp. Match 40	-	152.9	194.1		7.88	188.6		94.5	

Beyond the specific materials tested in this work, it is of interest to test other hcp metals (Ti alloys) and steel alloys using the meso-scale methodology to assess electric current effects on plastic deformation. Further in situ TEM experiments as outlined in Chapter 2 on additional materials with differing crystal structures (i.e., bcc and hcp) would be extremely beneficial to map the possible boundary diffusion and other electron-lattice interactions at play.

CHAPTER 4: CONCLUSIONS AND RECOMMENDATIONS

Electrically assisted deformation (EAD) has been proposed for enhancing the formability of metals through electric current-induced reductions in flow stress and ultimate strength. Despite its potential for manufacturing applications and many years of research, the role of the two key proposed mechanisms, intrinsically coupled electroplasticity (non-thermal effects) and resistive heating (thermal effects), has not been resolved. The primary technical challenges impeding progress have been: 1) developing critical experiments (methodology and hardware) capable of unambiguously separating the contributions of electric current and Joule heating to the plastic deformation process; and 2) the inherent complexity of the potential electric current interactions with the deformation processes in metals, which are governed by a diverse range of physical mechanisms, material properties, and microstructures.

The passage of electric current in a metal produces temperature increases via Joule heating, and temperature directly affects thermally-activated deformation mechanisms including thermal softening and expansion in metals that can significantly mask non-thermal (e.g., electron interactions) effects. Metals are comprised of many different crystal structures (i.e., fcc, bcc, and hcp) as well as microstructural features with length scales ranging from ~Å to ~μm (e.g., voids, dislocations, and grain boundaries), which give rise to a range of deformation mechanisms. Because of these complexities, thorough experimental studies on the individual and/or accumulative effects of the crystal- and micro-structures on EAD become non-trivial.

The development of robust and general techniques to characterize the plastic deformation behavior of metals with concurrent and accurate control of coupled electrical, thermal, and mechanical loadings is critical. The meso-scale testing methodology developed in this research carefully addressed many of the localized temperature and strain gradient issues that may have led to the proliferation of many differing results for tests on the same material [1, 20]. The experiments performed in this work unambiguously showed that the passage of electric current through pure Cu or Fe reduces the deformation forces, but the reductions are due to the increased temperature alone. The experiments with pure Ti discovered novel grain growth that only occurred with concurrent electric current (with accompanying temperature increases) and mechanical deformation. Mechanisms that might explain these findings are being explored and are expected to provide new insight on EAD of metals.

This research has provided a new capability for electromechanical testing of metals specimens at different length scales, i.e., ~μm and ~mm, which enable investigations of coupling between electric current and specific microstructures. As an example, we tested micro- and meso-scale specimens for electromechanical characterization of copper utilizing the two experimental approaches developed at NRL. The aim of the former was to directly answer how dislocations without grain boundaries respond to coupled electromechanical loading. This study explicitly showed that the mobility of dislocations remained unaffected by electric current densities up to 5000 A/mm^2. The meso-scale study included grain boundaries with the scaled-up specimen size, and this study showed that all observed changes in deformation behavior with electric current

were due solely to thermal effects. These two experimental results show that neither dislocation-electron interactions nor localized grain boundary heating result in electroplasticity of pure copper.

So far, the experimental approach for meso-scale specimens has been utilized for characterization of pure Cu, Fe and Ti. Among these, only the titanium showed a considerable reduction in flow stress due to electric current. This reduction, however, was coupled with grain growth that only occurred with concurrent electric current and mechanical deformation. Detailed in situ testing of titanium specimens with locally tailored microstructures, e.g., grain orientations and sizes, dislocation distribution, and other defects would pave new ways to validate the potential effects of current-microstructure interactions during material deformation. These fundamental in situ studies may provide deeper insights towards the development of effective electrically assisted deformation processes for advanced manufacturing as well as design of multifunctional materials for electromechanical applications.

REFERENCES

[1] C. D. Ross, T. J. Kronenberger, and J. T. Roth, "Effect of dc on the Formability of Ti-6Al-4V," (in English), *Journal of Engineering Materials and Technology-Transactions of the Asme,* vol. 131, no. 3, Jul 2009.

[2] F. Gallo, R. Watkins, K. Ravi-Chandar, and S. Satapathy, "Strain evolution in metal conductors subjected to short-duration current pulses," (in English), *Ieee Transactions on Magnetics,* vol. 43, no. 1, pp. 338-342, Jan 2007.

[3] K. Okazaki, M. Kagawa, and H. Conrad, "A Study of Electroplastic Effect in Metals," (in English), *Scripta Metallurgica,* vol. 12, no. 11, pp. 1063-1068, 1978.

[4] V. L. A. Silveira, M. F. S. Porto, and W. A. Mannheimer, "Electroplastic Effect in Copper Subjected to Low-Density Electric-Current," (in English), *Scripta Metallurgica,* vol. 15, no. 8, pp. 945-950, 1981.

[5] M. S. Siopis and B. L. Kinsey, "Experimental Investigation of Grain and Specimen Size Effects During Electrical-Assisted Forming," (in English), *Journal of Manufacturing Science and Engineering-Transactions of the Asme,* vol. 132, no. 2, Apr 2010.

[6] J. S. Andrawes, T. J. Kronenberger, T. A. Perkins, J. T. Roth, and R. L. Warley, "Effects of DC Current on the Mechanical Behavior of AlMg1SiCu," *Materials and Manufacturing Processes,* vol. 22, no. 1, pp. 91-101, 2007.

[7] R. Fan, J. Magargee, P. Hu, and J. Cao, "Influence of grain size and grain boundaries on the thermal and mechanical behavior of 70/30 brass under electrically-assisted deformation," *Materials Science and Engineering: A,* vol. 574, pp. 218-225, 2013.

[8] A. Khalilollahi, D. H. Johnson, and J. T. Roth, "A Comparative Multifield FEA and Experimental Study on the Enhanced Manufacturability of 6061-T6511 Aluminum Using dc Current," (in English), *Journal of Manufacturing Science and Engineering-Transactions of the Asme,* vol. 131, no. 6, Dec 2009.

[9] T. A. Perkins, T. J. Kronenberger, and J. T. Roth, "Metallic forging using electrical flow as an alternative to warm/hot working," (in English), *Journal of Manufacturing Science and Engineering-Transactions of the Asme,* vol. 129, no. 1, pp. 84-94, Feb 2007.

[10] W. A. Salandro, C. J. Bunget, and L. Mears, "Several Factors Affecting the Electroplastic Effect During an Electrically-Assisted Forming Process," (in English), *Journal of Manufacturing Science and Engineering-Transactions of the Asme,* vol. 133, no. 6, Dec 2011.

[11] K. Okazaki, M. Kagawa, and H. Conrad, "Study of Electroplastic Effect in Metals," (in English), *Scripta Metallurgica,* vol. 12, no. 11, pp. 1063-1068, 1978.

[12] W. Kang, I. Beniam, and S. M. Qidwai, "An In Situ TEM Study of the Electromechanical Behavior of Metals Using an Innovative Micro-Device Testing Method," in *International Congress of Theoretical and Applied Mechanics*, 2016.

[13] R. C. Reid, A. Pique, and W. Kang, "A Novel Method for In Situ Electromechanical Characterization of Nanoscale Specimens," (in English), *Jove-Journal of Visualized Experiments,* no. 124, Jun 2017.

[14] W. Kang, I. Beniam, and S. M. Qidwai, "In situ electron microscopy studies of electromechanical behavior in metals at the nanoscale using a novel microdevice-based system," (in English), *Review of Scientific Instruments,* vol. 87, no. 9, Sep 2016.

[15] J. T. Roth, I. Loker, D. Mauck, M. Warner, S. F. Golovashchenko, and A. Krause, "Enhanced Formability of 5754 Aluminum Sheet Metal Using Electric Pulsing,"

presented at the Transactions of the North American Manufacturing Research Institution of SME, 2008.

[16] J. J. Jones, L. Mears, and J. T. Roth, "Empirical Modeling of the Stress-Strain Relationship for an Upsetting Process Under Direct Electrical Current," presented at the Transaction of the North American Manufacturing Research Institute of SME, 2010.

[17] J. Magargee, F. Morestin, and J. Cao, "Characterization of Flow Stress for Commercially Pure Titanium Subjected to Electrically Assisted Deformation," (in English), *Journal of Engineering Materials and Technology-Transactions of the Asme,* vol. 135, no. 4, Oct 2013.

[18] T. H. Jiang, L. F. Peng, P. Y. Yi, and X. M. Lai, "Investigation of Deformation Behavior of SS304 and Pure Copper Subjected to Electrically Assisted Forming Process," (in English), *Journal of Manufacturing Science and Engineering-Transactions of the Asme,* vol. 139, no. 1, Jan 2017.

[19] C. D. Ross, D. B. Irvin, and J. T. Roth, "Manufacturing aspects relating to the effects of direct current on the tensile properties of metals," (in English), *Journal of Engineering Materials and Technology-Transactions of the Asme,* vol. 129, no. 2, pp. 342-347, Apr 2007.

[20] B. Kinsey, G. Cullen, A. Jordan, and S. Mates, "Investigation of electroplastic effect at high deformation rates for 304SS and Ti-6Al-4V," (in English), *Cirp Annals-Manufacturing Technology,* vol. 62, no. 1, pp. 279-282, 2013.

APPENDIX A: STITCHED TITANIUM MICROSTRUCTURE IMAGES

The following images are stitched microstructure images from some of the titanium specimens tested at the listed conditions. The images are stitched from the neck (left side) to ~6 mm away from the neck.

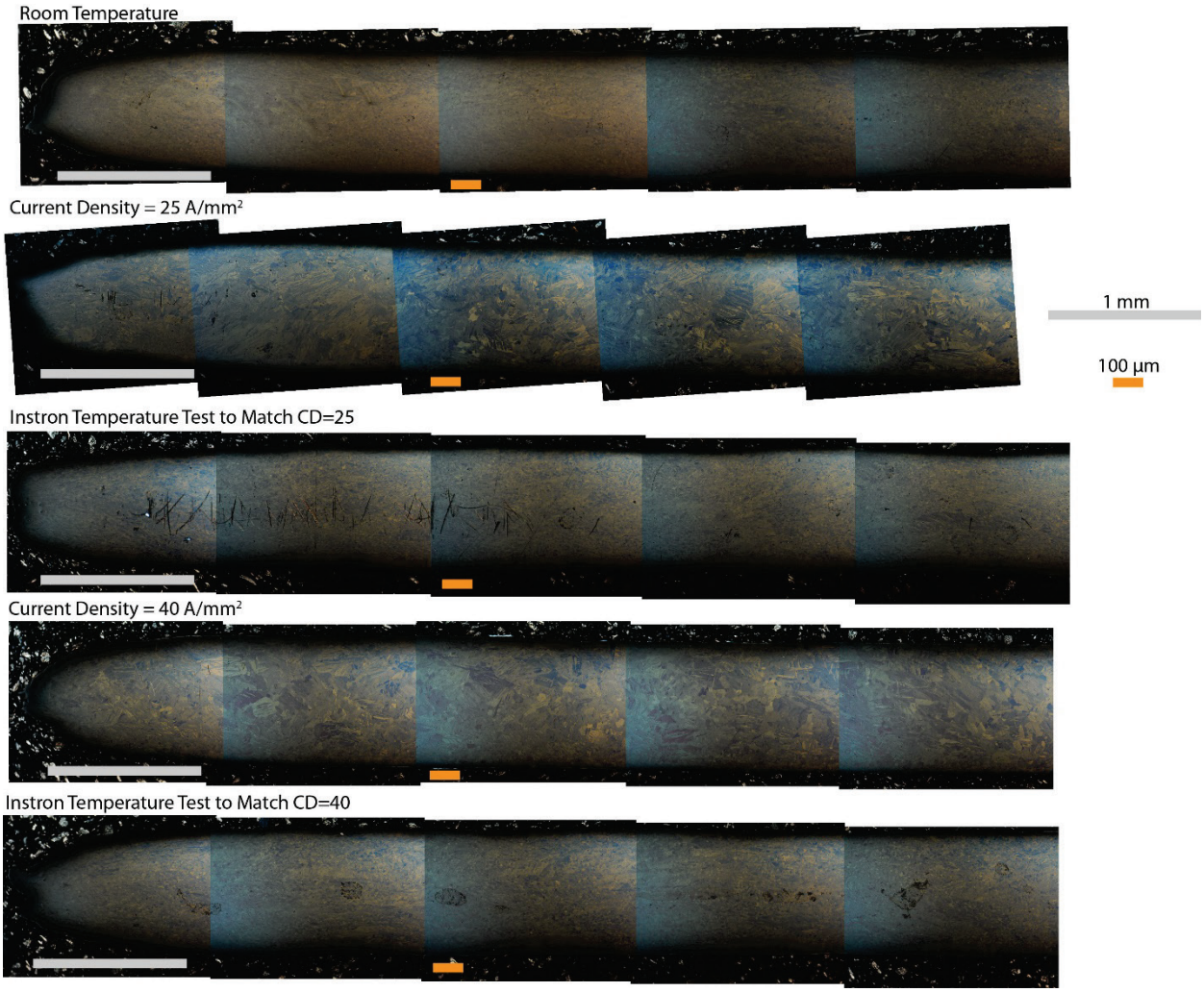

Figure 15: Stitched microstructure images of tested Ti specimens from necking location (left).

APPENDIX B: MESOSCALE TEST SYSTEM DEVELOPMENT

The initial plan for the meso-scale experimentation was to develop the capability for performing in situ SEM electromechanical testing[1]. A SEMTester Model 2000 EBSD was purchased, and modifications were made to enable electrical current through the specimen under test. This device came with loading fixtures for tensile, compression, and bend testing, and the maximum specimen size that can be tested is: 64 mm (L) x 10 mm (W) x 2.5 mm (T). The range of possible gage lengths is considerably smaller after gripping and material strain extensions during testing are considered.

The critical requirement for this test system design was to achieve uniform current, temperature and strain conditions in the specimen gage section (prior to specimen necking). Due to the small specimen size, the electric current had to be applied through the specimen grips. Only the tensile loading-mode offered the possibility of achieving uniform conditions in the gage section. That is, only in tension is the gage section large enough to provide a dominate response behavior relative to concentration effects at the specimen-grip interface.

In order to simulate SEM operational conditions, the SEMTester was mounted inside of a benchtop vacuum chamber. This chamber had appropriate electrical, gas, and fluid feedthroughs and a polycarbonate window on top to allow non-contact video strain measurements (Figure 16). Operating with the device in the chamber presented significant challenges, particularly in terms of mounting specimens. The current/ground connections inside of the chamber were essentially fixed, so the SEMTester could not be easily removed and returned for specimen mounting. Strain measurements in the SEM would have to be inferred from cross-head displacements (non-ideal), or by video extensometry if SEM chamber had a window and the device could be oriented to provide a direct specimen gage view.

Test system design to achieve the desired specimen currents was a challenge. Current densities, j, as high as several hundred A/mm^2 were desirable. The current, I, needed is dictated by the specimen cross-section area. For example, using the maximum specimen cross-section (25 mm^2) and assuming j = 100 A/mm^2 requires a 2500 A current! Clearly, specimens much smaller in size are needed!

The SEMTester provides wedge-loaded grips for tensile loading of flat (sheet) specimens. Dogbone specimens were developed over several iterations (see the Specimen drawings below). A final design (Dogbone 003) had the gage dimensions: 8.75 mm length, 1.50 mm width, and 1.00 mm thickness. This 1.50 mm^2 cross-section area would need 150 A for a current density of 100 A/mm^2, and working with this level of current was feasible. A current supply capable of 440 A (HP Model 6690A) was purchased.

The SEMTester and tensile-grip fixturing had to be modified to safely provide several hundred amps passing through the test specimen. The grip with the positive current connection (load application grip) would have to be electrically isolated from the rest of the device and capable of carrying the maximum tensile load. It was decided to also electrically isolate the (earth) ground grip (fixed load-cell grip) so that no current could pass through the load cell. Numerous earth ground cables were added to the device for safety (see Figure 16). The electrical isolation hardware for the wedge grips had to be mechanically robust enough to handle the maximum mechanical loads. In addition, this MTI Instruments device, Model 2000 EBSD, was designed to allow specimen rotation for EBSD analysis in the SEM. That is, the wedge

[1] A critical question arose as to whether SEM imaging would even be possible in this experiment with large currents flowing through the specimen due to the circumferential magnetic field that would develop. We never got far enough with the system development to test this hypothesis.

grips could rotate about the loading axis. This complicated the grip isolation-load hardware design. The tensile wedge grip hardware was reverse-engineered to generate new CAD-machining drawings (MTI would not provide drawings). The grip feature dimensions were modified to accommodate electrical isolation sleeves and washers made of polyimide and phenolic materials. The insulation hardware provided electrical isolation of the tensile wedge-grips and specimen from the rest of the SEMTester device while also being capable of transmitting tensile loads to grips and specimen.

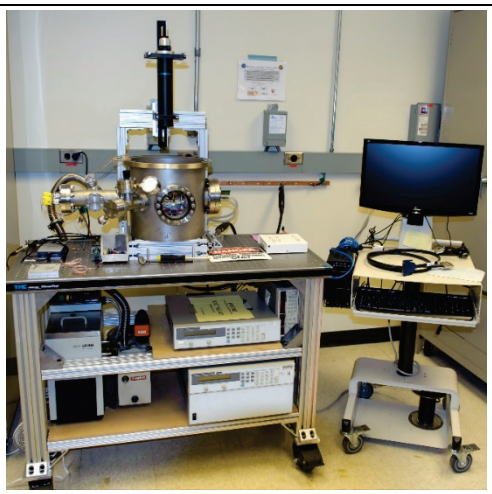

(a)

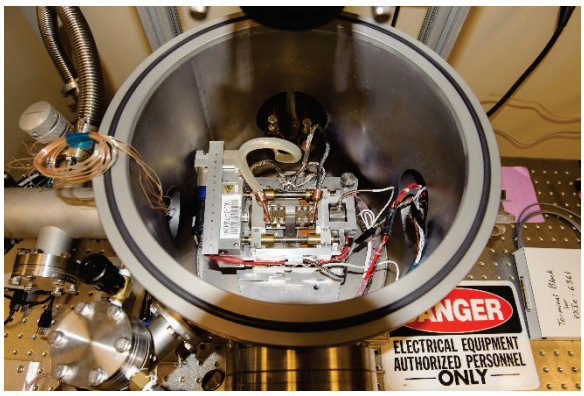

(b)

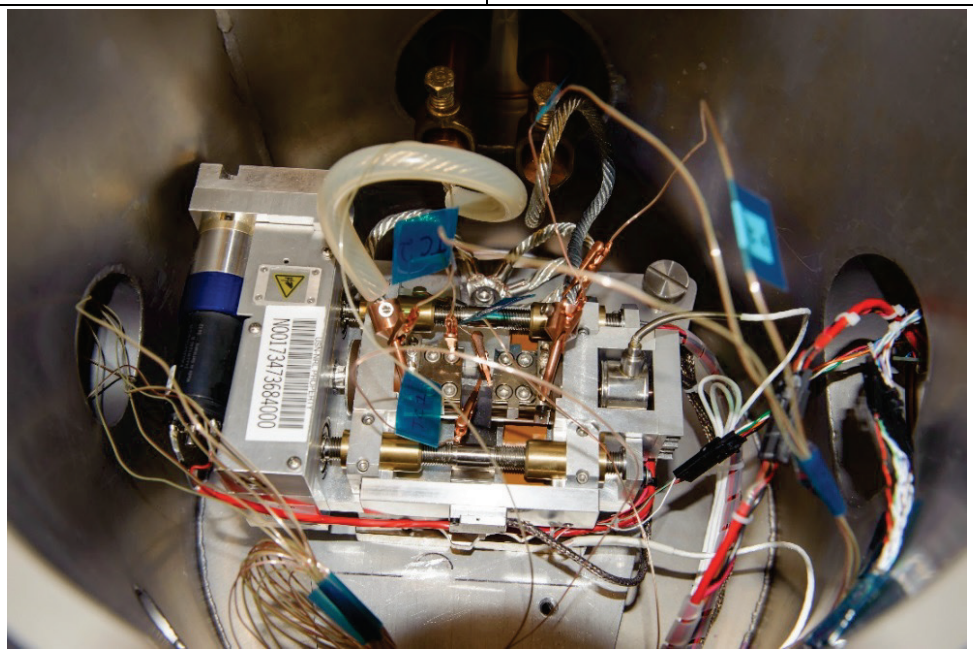

(c)

Figure 16: Earliest meso-scale test system that was designed for vacuum-chamber SEM operation. (a) Table-top vacuum chamber with instrumentation and computer for data acquisition; (b) current supply and load-frame ground lead connections inside the chamber; (c) load-frame with a dogbone specimen inserted and multiple attached thermocouples.

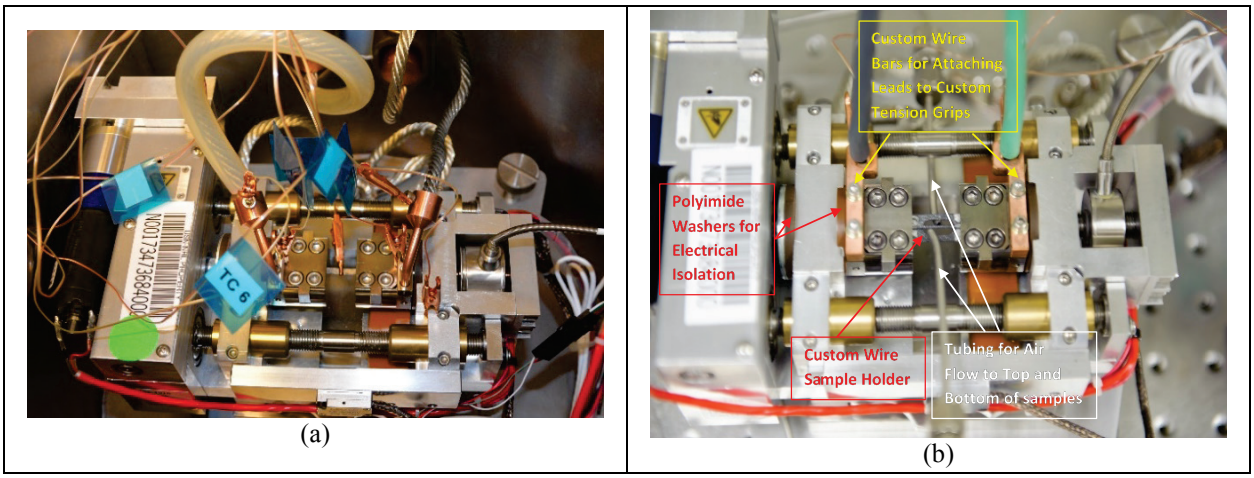

(a) (b)

Figure 17: (a) original wire bus bar design for current passage and (b) finalized design used to pass current through specimens on the SEMTester loading stage.

The next design challenge was to connect current supply leads to the wedge-grips. The initial design, shown in Figure 17a and Figure 16 consisted of a Cu bar fastened to the grip and a Cu adapter to transition from the large braided Cu (3 Ga) supply cables to a smaller diameter solid Cu grip attachment wire. The multiple electrical connections in this design had contact resistances large enough to produce excessive heating so a revised design was developed. It consisted of a Cu bus-bar fastened to each wedge grip that extended with a hole for attaching a smaller braided-Cu (6 Ga) lead (see Figure 26, Figure 17b). This connector design, used in all subsequent testing, functions very well with minimal increases in the connector temperature at high currents (several hundred amps).

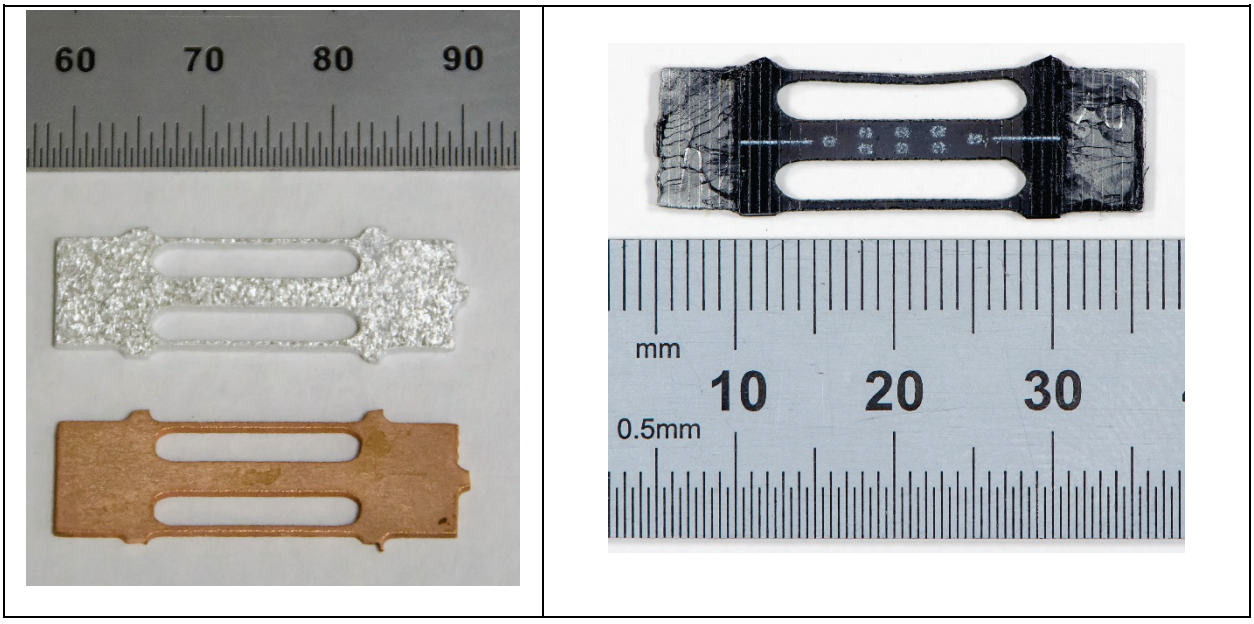

Figure 18: (Left) pure Al and Cu tensile specimens (mm scale shown). (Right) aluminum tensile specimen with high-emissivity (black) graphite coating for IR spot temperature measurements and white circle targets for axial and transverse non-contact video strain measurements.

The load cell on the SEMTester had an 1100 N (250 lbsf) capacity. The cross-section area of the tensile test specimen was designed to reach ultimate failure stresses at loads below the load cell capacity and the desired current density levels with currents less than 150-200 A for the metals of interest. A simple design plot was generated for applied stresses at the 1100 N load cell force capacity and for current densities at 10 A as a function of the test specimen cross-section area (see Figure 19 below). The dogbone specimens had a cross-section area of 2.5 mm^2, and for this size, the maximum possible applied stress at 1100 N was 445 MPa; the current density for 10 A current was 4 A/mm^2. This implied that the material under test should have an ultimate strength less than the 445 MPa, and 100 A/mm^2 current density would require 250 A of current. The maximum stress possible and the current levels needed for desired current density levels led to the decision to further reduce the gage cross-section.

Circular wire specimens nominally 1 mm in diameter were selected for simplicity (no machining needed) and the ready availability of high-purity materials in this configuration. For 1 mm diameter circular cross-sections, the maximum possible stress in the specimen at 1100 N load is 1410 MPa, which exceeds the ultimate strength of most pure and alloy metals. The corresponding current density at 10 A current is 12.7 A/mm^2, so a specimen current density of 100 A/mm^2 would require only ~80 A of current, a threefold reduction from previous dogbone specimens.

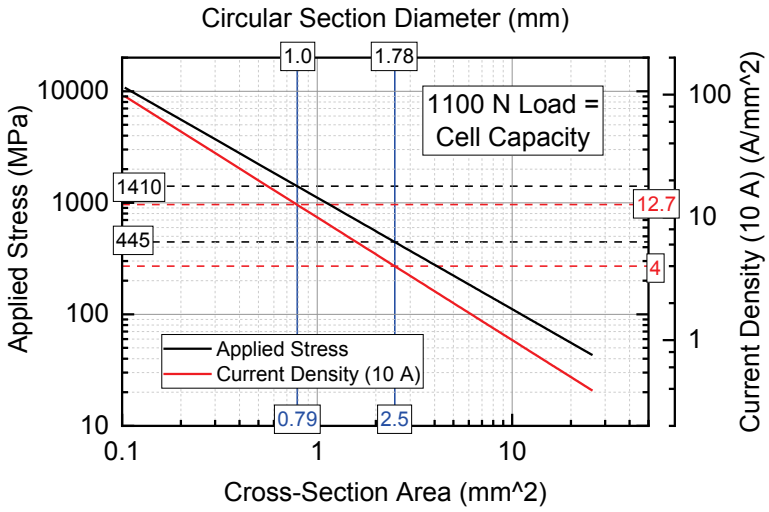

Figure 19: Specimen sizing design plot.

The switch to this new wire geometry required consideration of interfacing the specimens with flat wedge grips. Simply clamping the wire with flat wedges would crush the wire leading to failure in the grips. In addition, significant electrical and thermal contact resistances would lead to excessive specimen heating, especially at the specimen-grip interface. Several tabbing options were developed to address these issues. The first tab design shown in Figure 20 had a groove for the centering wire ~50% larger than the wire diameter. Only a single tab was used, and a small piece thin Cu shim stock was placed over the top of the specimen to better distribute the loads and assist in current and thermal transfers to the grip (Figure 21). This design did not work well, and a new tab was designed (Figure 22 and Figure 23; also see Figure 29 thru Figure 32). These new tabs had circular grooves ~2% larger in diameter than the wires, but a slightly reduced depth. Two tabs were used in this design to sandwich the wire specimen, and these tabs worked quite well showing good load transfer, failure in the gage section, and significant gage section temperature reductions through grip-conduction.

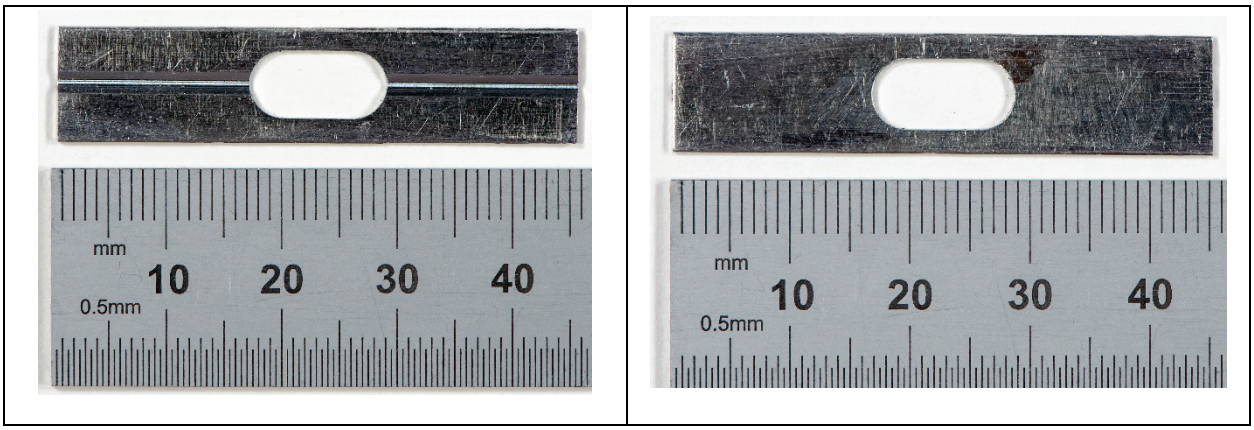

Figure 20: Photos of the original tab designs for the wire specimens. A single tab was used with each wire specimen, and the wire groove radius was ~50% larger than the radius.

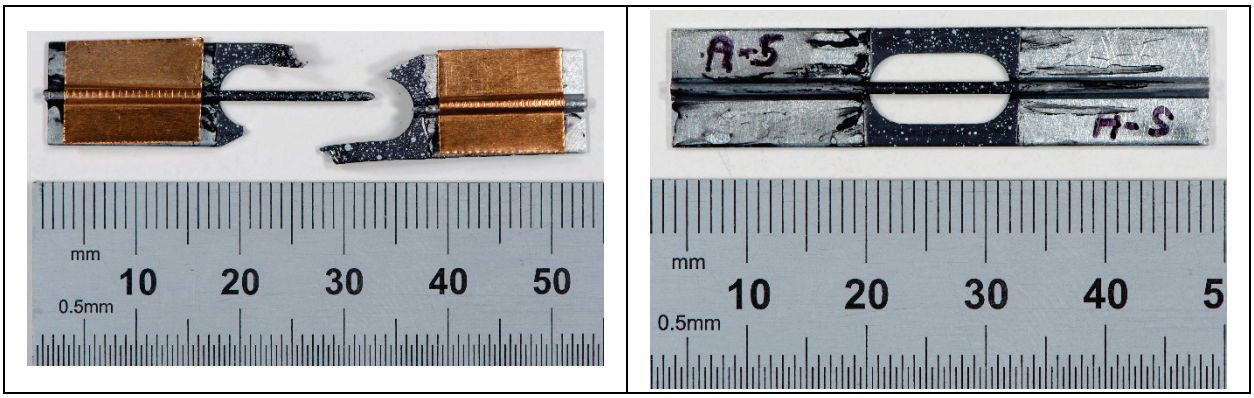

Figure 21: Photos of the original tab designs with (left) Cu shim-stock load/thermal spreader pads and (right) pure-Al wire with black graphite IR emissivity coating and white speckles for strain measurement.

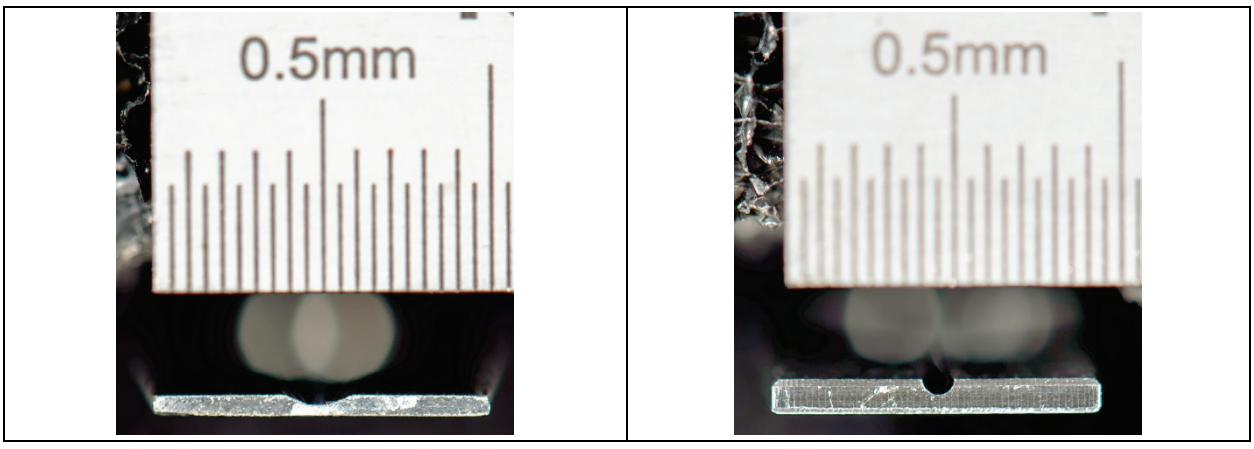

Figure 22: Photos of the (left) original and (right) final tab cross-sections showing the different wire specimen contact zone radii.

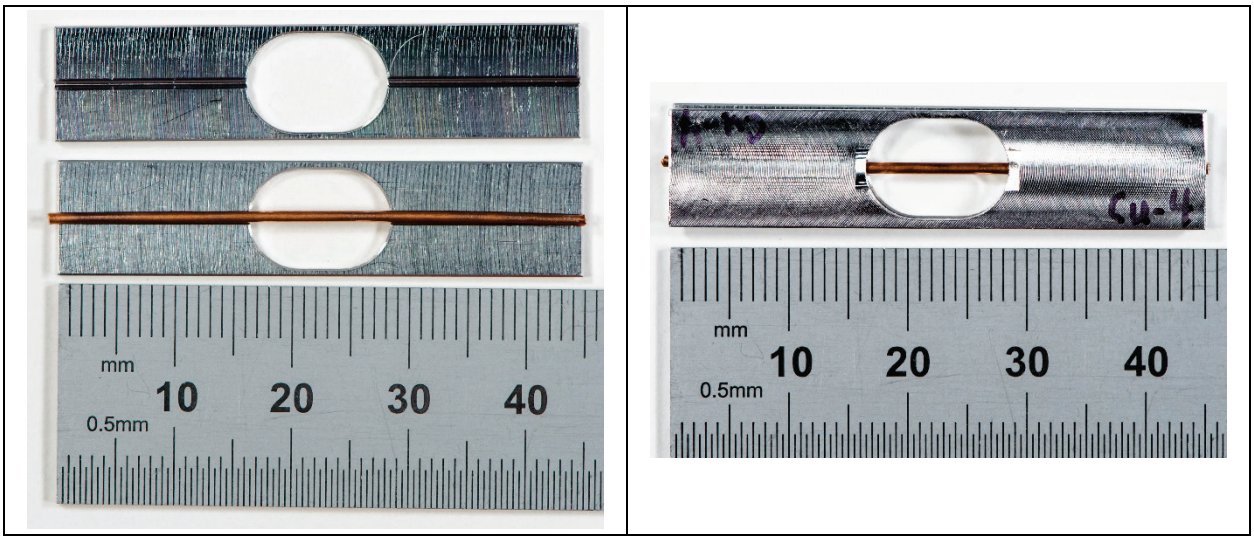

Figure 23: Photos of the final tab design with a Cu specimen before and after clamping the two halves together.

Attempts were initially made to measure gage section temperatures using thermocouple (TC) wires welded to the original dogbone specimens or attached via small Cu alligator clips. Neither approach worked due to welding difficulties, and specimen size/handling constraints. The use of Micro-Epsilon IR spot-temperature sensors was considered next: 1) CTLM-3LCF3-C3, 50°C to 400°C, 3.3 mm spot-size; and 2) CTLM-3HCF3-C3, 100°C to 600°C, 2.0 mm spot size. These were difficult to calibrate, and ultimately, would provide temperatures at one or two points on the specimen. Real-time assessment of temperature uniformity along the gage length would not be possible.

The transition from dogbone to circular wire specimens made temperature measurements even more challenging. A full-field, non-contact, video IR temperature measurement system was eventually procured to accurately measure temperatures along the specimen gage section during testing.

The final design issue was specimen cooling. Such large current densities will naturally lead to large increases in specimen temperature through Joule heating. With natural convection, or radiative heat transfer (in the SEM vacuum) the middle point of the specimen gage length will reach the highest temperature since this point is furthest from the cooler (large mass) grips. In addition, metal surfaces have relatively low surface emissivity, and the heat flow rate by radiation transfer is directly proportion to surface emissivity. There are graphite coatings that can be applied to increase the emissivity, but then nothing could be seen in the SEM. Clearly, performing coupled electromechanical testing in the SEM would only be possible with very low current densities. Additionally, the temperature in the gage section would need to be as uniform as possible and as small as possible for any given applied current. This is required to effectively de-couple Joule heating from electric current effects on the mechanical deformation behavior. The only conclusion is that active cooling of the specimen would be necessary if larger test current densities were to be used!

Multiple methods for actively cooling the specimen were attempted. The first approach, one that might still be compatible with some specialized form of SEM, was to conduct the test with a He gas atmosphere and He flows convectively cooling the gage section (see Figure 26). Helium gas was selected due to its relatively high thermal conductivity. This approach was possible with the SEMTester housed within the benchtop vacuum chamber. This did not lead to an appreciable improvement in specimen cooling. The

next approach was to remove the SEMTester from the vacuum chamber and perform the tests in open lab atmosphere on the benchtop.

Convective N_2 cooling was used at much higher flow rates, which showed better cooling (lower overall specimen temperatures) and smaller improved temperature gradients along the specimen length. Also, open-top access to the SEMTester on the benchtop really helped simplify the testing and sample mounting processes. Average specimen temperature increases still led to limitations on the current density levels possible with each material type. Bottled N_2 gas streams were impinged on the specimen gage length through two small diameter stainless steel tubes venting on the specimen from the front and back. Given the length of the test and the limited amount of starting nitrogen, the N_2 pressure regulator could be set at no more than 15-20 psi. This setup worked well for cooling high conductivity (i.e. Cu) samples; they were cooled from >50°C without external cooling at 30 A/mm^2 to ~25 °C with cooling. This approach was not capable of cooling the lower conductivity specimens at higher current densities, and it was abandoned. The N_2 nozzles were used, however, to provide auxiliary cooling of the grips and electrical leads for the high current tests (e.g., 200 A/mm^2 on copper).

To address some of the concerns about torsional stress and the required electric currents, it was decided that 1 mm diameter wires would be a better sample geometry. This resulted in a cross-sectional area reduction from 1.5 mm^2 (Dogbone 003) to 0.785 mm^2. A key challenge in testing uniform 1 mm wire samples in tension was how to grip the wire and achieve failure in the gage-section. The initial wire specimen holder design (holder 001, Figure 24a) was a simple, one-sided v-groove tab holder machined from aluminum. The wire was engaged by the wedge grips of the testing apparatus on top and the aluminum tab holder on the bottom. Like the dogbone specimen design, the wire tab holder has "outriggers" for alignment during mounting which were cut just prior to testing. This design did not allow the sample to break in the gage section as desired and the temperature was difficult to control due to uneven electrical resistance.

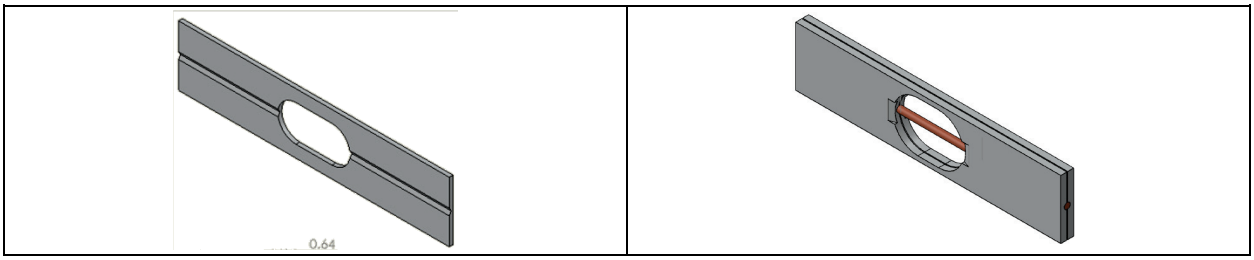

Figure 24: CAD images of wire holder tab designs: (a) holder 001 and (b) holder 002.

New wire sample holders made from aluminum were machined and tested for both the MTI SEMTester and Instron temperature-matched experiments. Wire holder 002 (Figure 24b) was more of a rounded design with a hemispherical groove down the center just lager than 1mm (1.16 mm) and just under 0.5 mm in depth (0.44) giving ~0.12mm gap when the wire is sandwiched between 2 of the machined bars. A channel was cut on the back of the plate where the wire is sandwiched to provide a stress transition as the wire is pressed between the plates within the wedge grips. This design resulted in better electrical contact with the grips, showing a ~10 deg C decrease in temperature rise at the 30 A/mm^2 level on copper and aluminum (Figure 25). After a slight loosening of the fixed side of the grips to allow self-alignment of the sample, this holder design resulted in sample failure in the gage-section. It should be noted that due to the fine surface finish on both the machined channels and the wire, slipping would occur between the wire

and tab holder. This was simply fixed by cutting 0.001” brass shims to the dimensions of the gripped area and inserting them between the wire and tab holder on one side only.

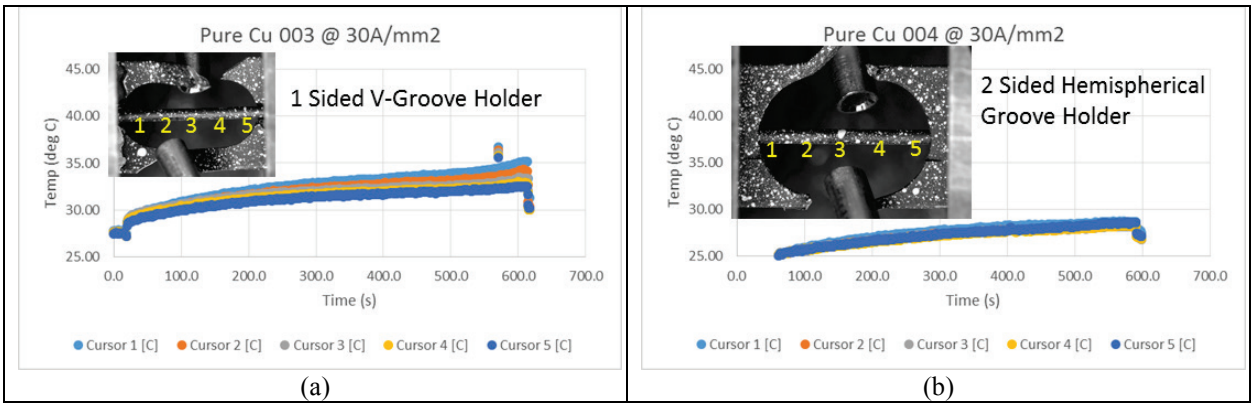

Figure 25: Comparative plots of temperature across wire samples for (a) holder 001 and (b) holder 002.

The wires are coated in their gage section with a thin layer of graphite black that produces an emissivity close to 1.0 for the accurate IR temperature measurement. A random speckle pattern of small white heat-resistant paint is sprayed on to enable to video extensometer to track points on the surface during testing for accurate axial and lateral strain measurements.

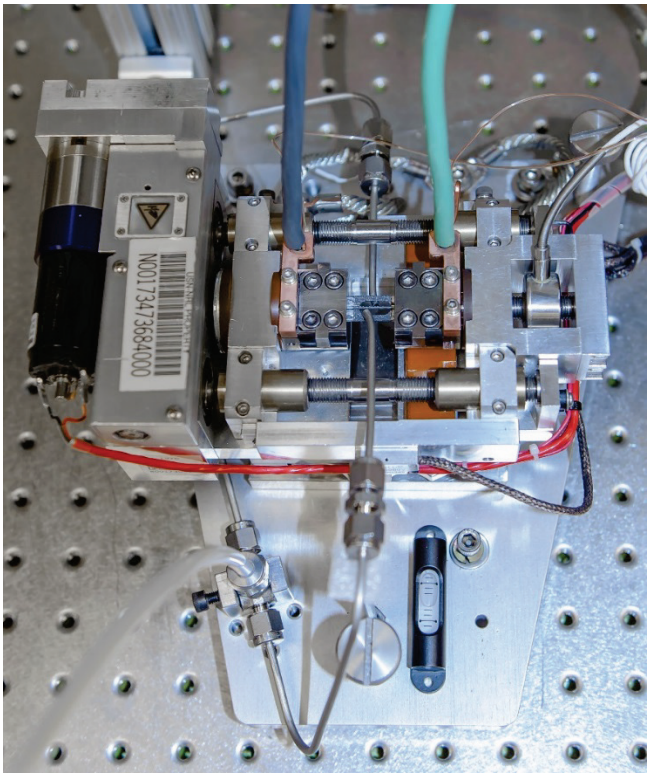

Figure 26: Meso-scale load-frame with the earlier N_2 gas nozzles for cooling. The tabbed specimen is visible (prior to cutting the tab out-riggers) along with current connections to the grips and insulating washers (brown).

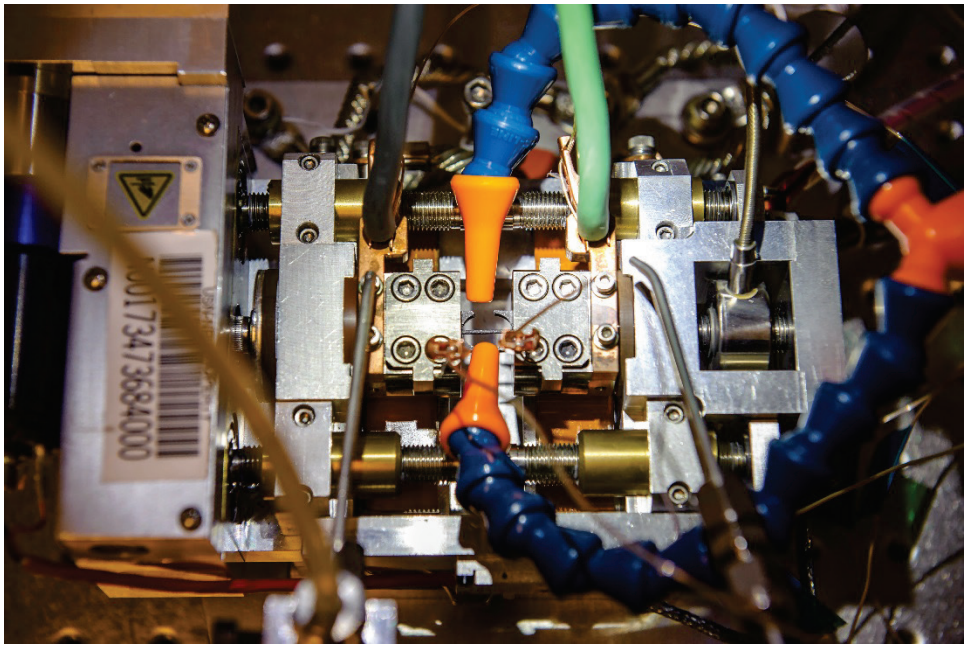

Figure 27: Final configuration of the meso-scale load-frame with the specimen being cooled by air via two venturi-nozzles with spreaders (orange), and two N_2 tube-nozzles for cooling the current-grip connections.

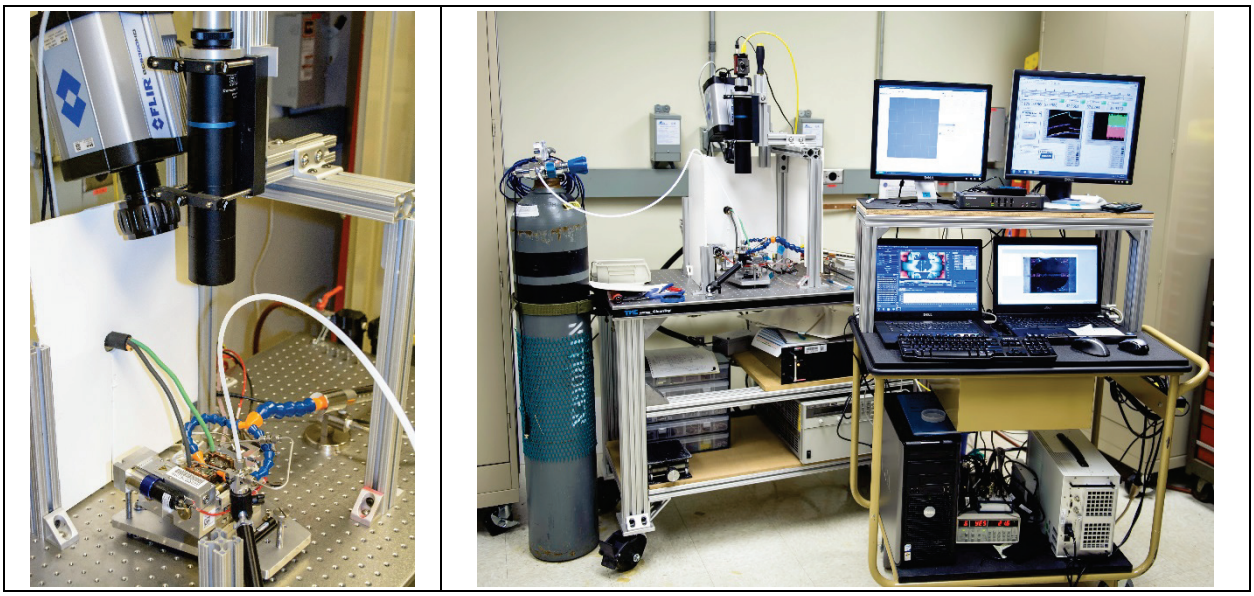

Figure 28: Meso-scale electro-thermo-mechanical test system. (Left) FLIR IR camera for temperature measurements, and MTS AVX video, non-contact strain measurement camera with a telecentric lens, and (right) overall view of the system showing the various control, data acquisition, and test instrumentation.

Specimen, Tab, and Fixture Drawings:

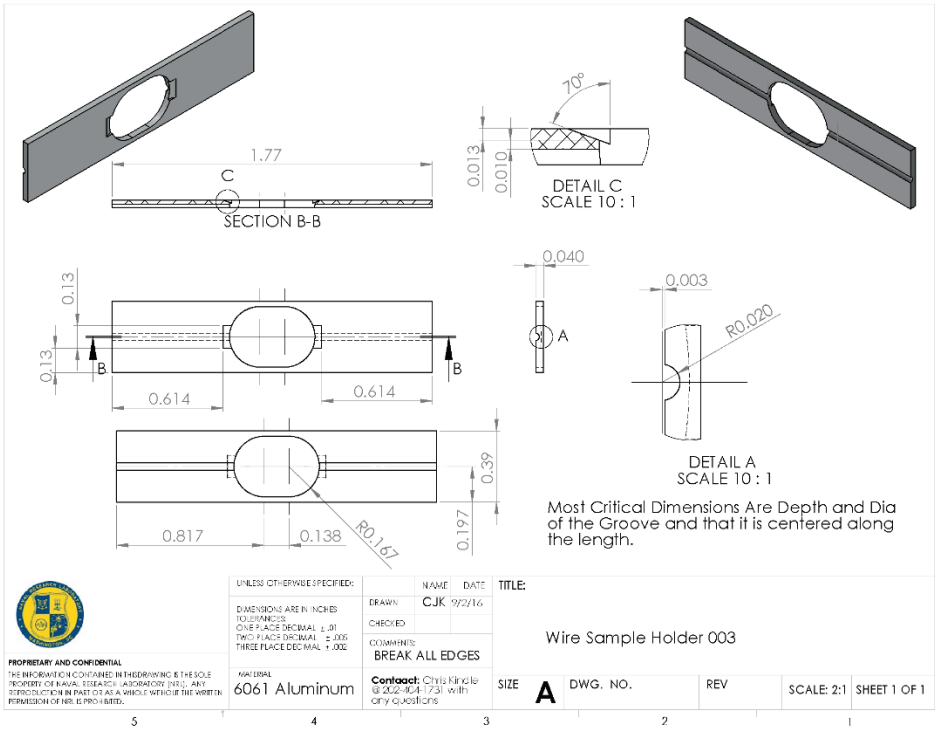

Figure 29: Machining drawing for the final tab design for the SEMTester wire tensile specimens.

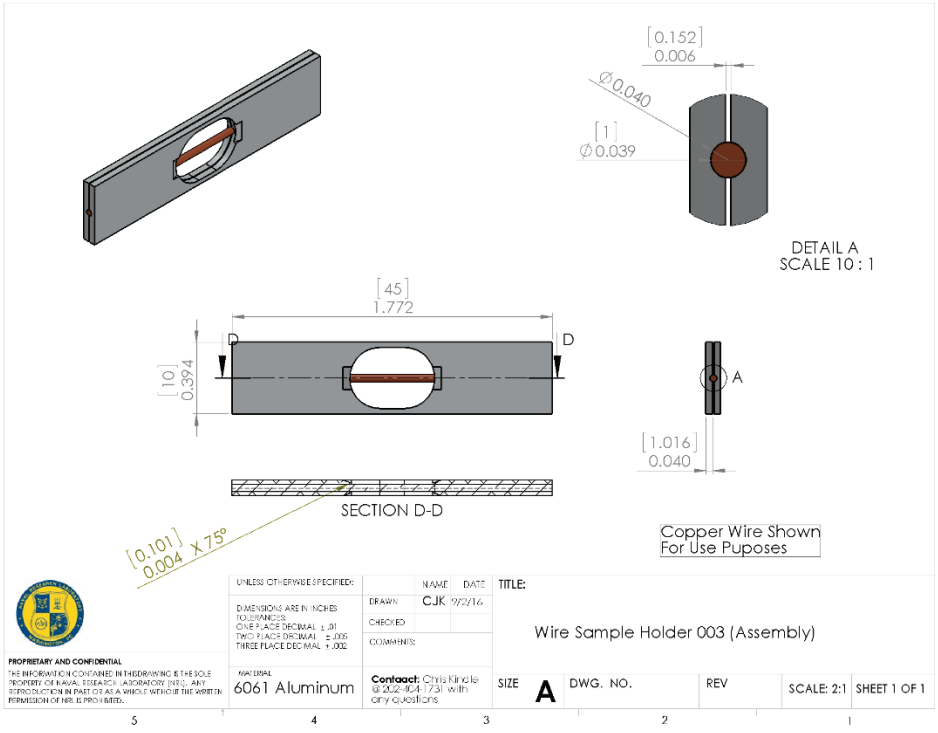

Figure 30: Tab-specimen assembly drawing.

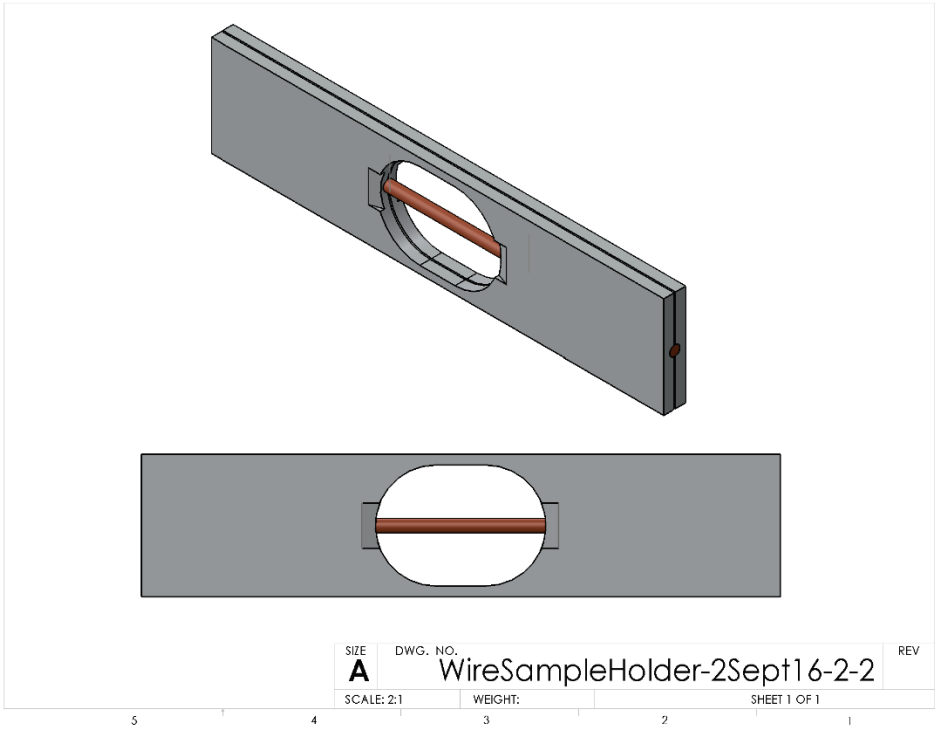

Figure 31: 3D view of a tabbed specimen.

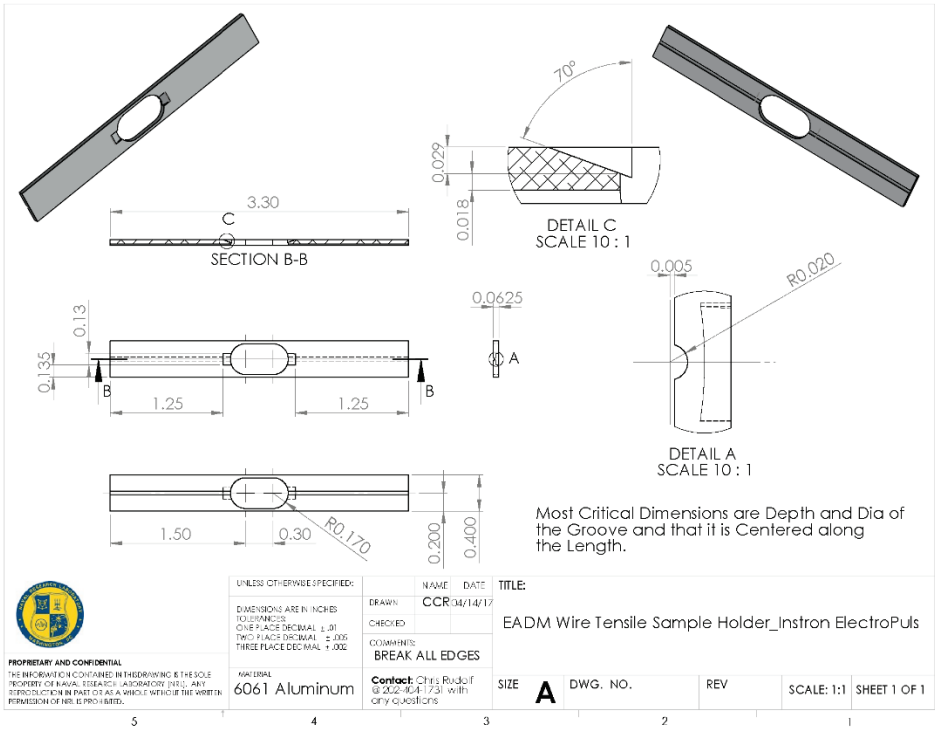

Figure 32: Machining drawing for specimen tabs with a larger gage-section and wedge-grip contact regions. The smaller SEMTester tabs were actually used in all of the Instron ElectroPuls baseline temperature response tests.

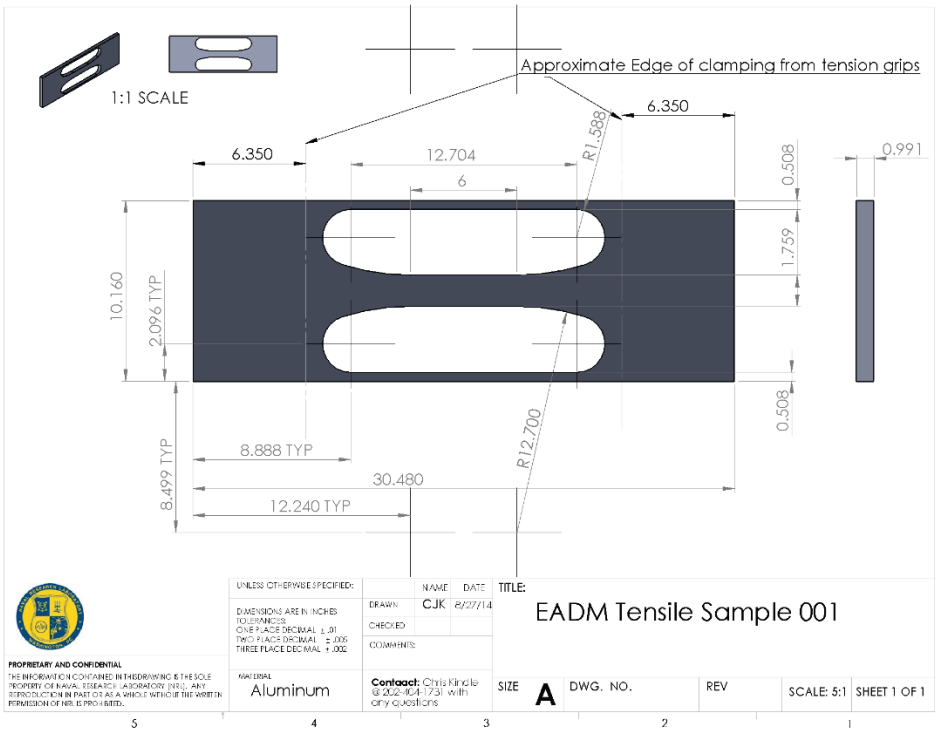

Figure 33: First dogbone specimen design (Dogbone 001).

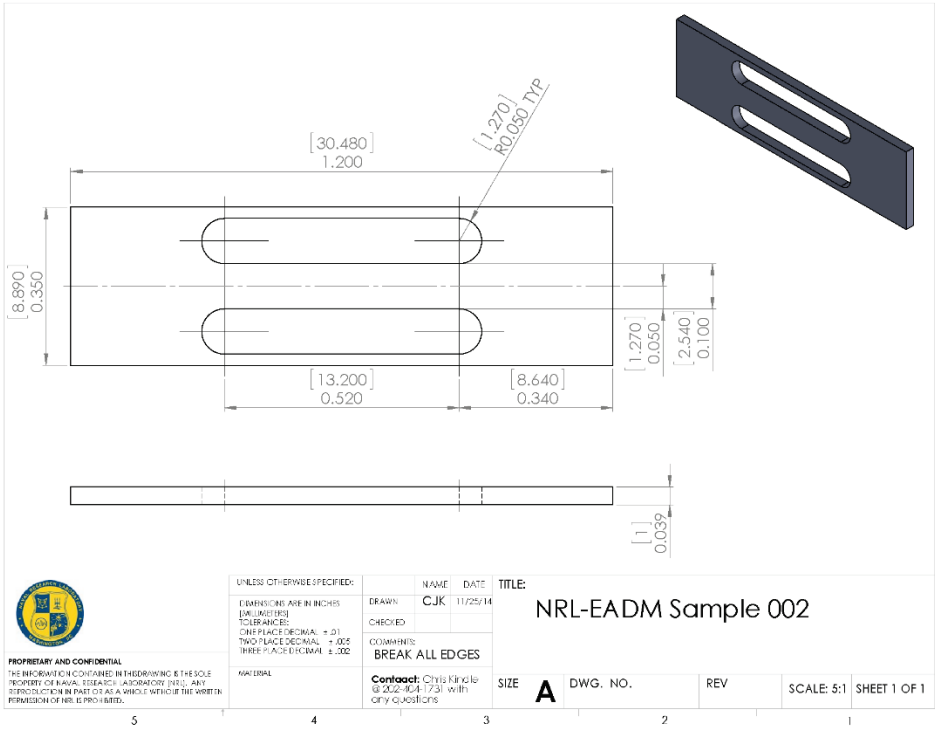

Figure 34: Second dogbone specimen design (Dogbone 002).

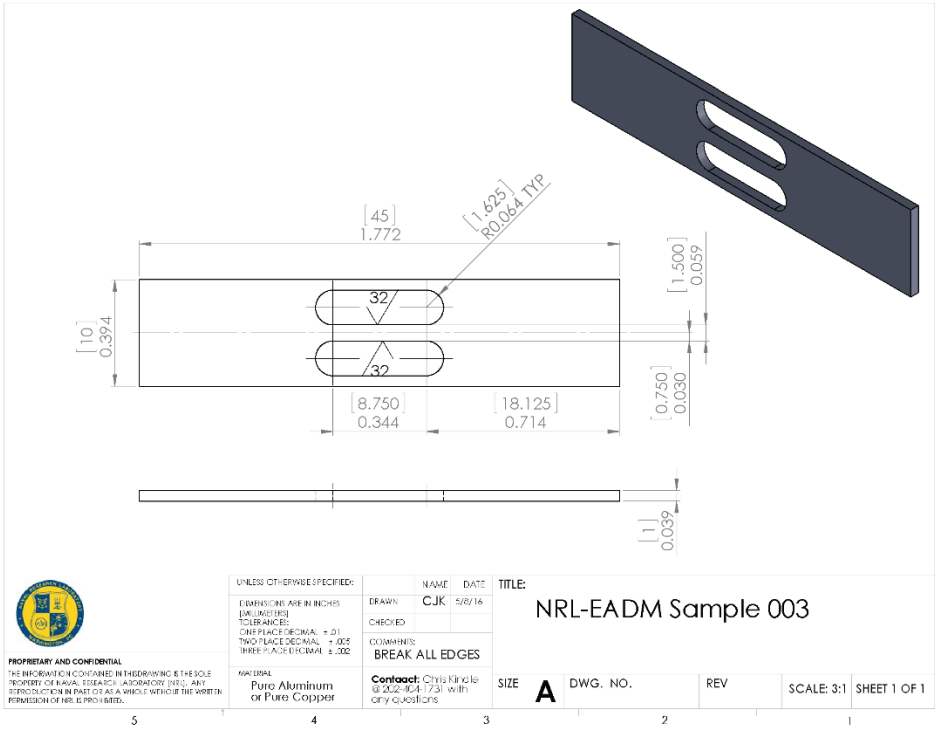

Figure 35: Final dogbone specimen design (Dogbone 003).

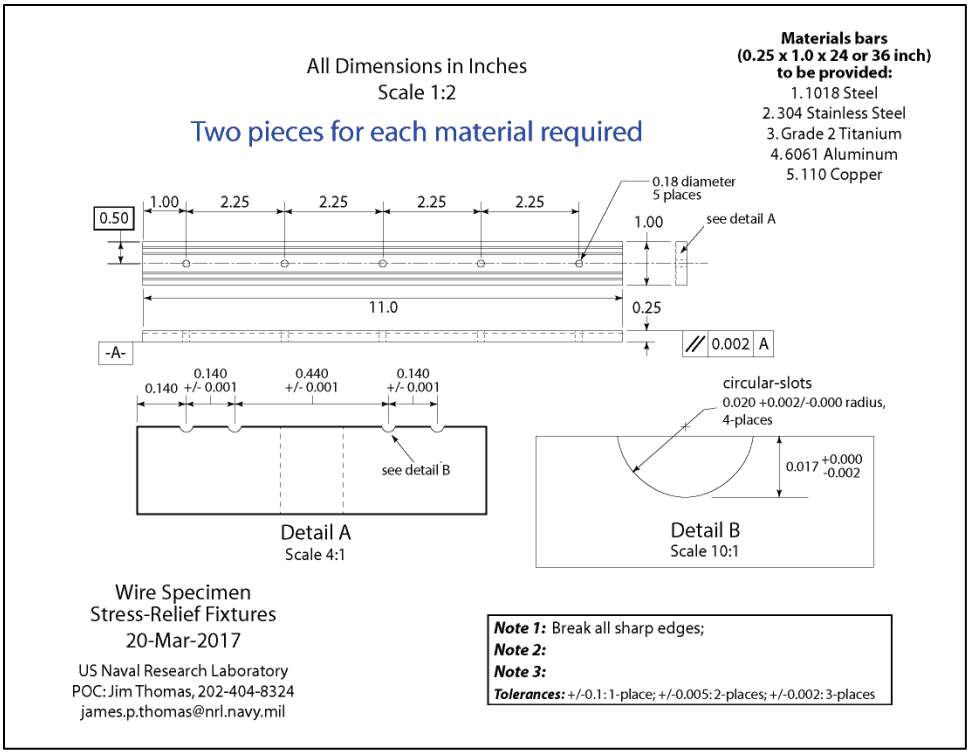

Figure 36: Machining print for the wire stress-relief/straightening fixtures.